AD-A186 689 PREDICTING DYNAMIC SEPARATION CHARACTERISTICS OF GENERAL CONFIGURATIONS(U) ANALYTICAL METHODS INC REDMOND WA B MASKEW ET AL. JUL 87 AMI-8706 1/1

UNCLASSIFIED AFOSR-TR-87-1418 F49620-82-C-0033 F/G 1/1 NL

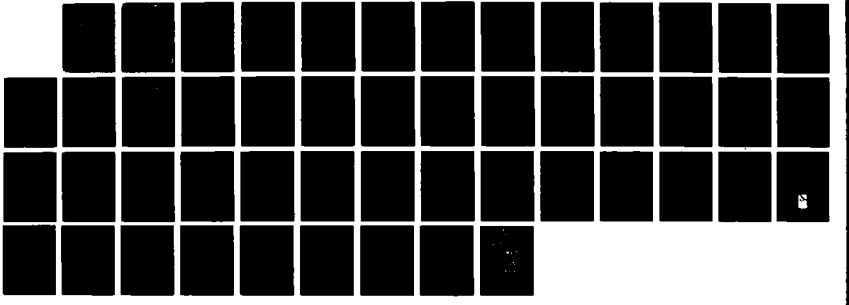

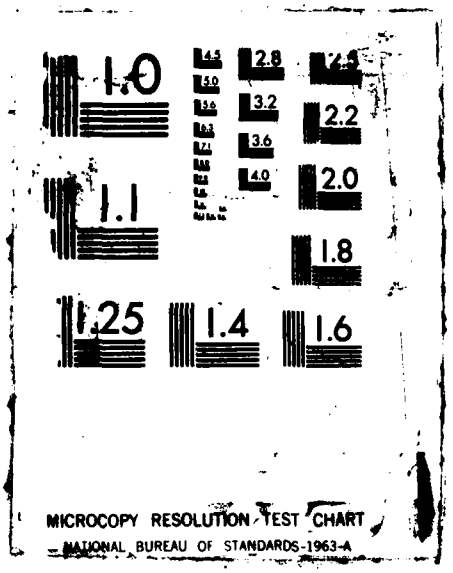
1.0
1.1
1.25
1.4
1.6
1.8
2.0
2.2
2.8
3.2
3.6
4.0
MICROCOPY RESOLUTION TEST CHART
NATIONAL BUREAU OF STANDARDS-1963-A

UNCLASSIFIED
SECURITY CLASSIFICATION OF THIS PAGE

DTIC FILE COPY

ORT DOCUMENTATION PAGE

1 **AD-A186 689**

1b. RESTRICTIVE MARKINGS

2 3 DISTRIBUTION/AVAILABILITY OF REPORT
Unlimited
Approved for public release; distribution unlimited.

2b. DECLASSIFICATION/DOWNGRADING SCHEDULE

4. PERFORMING ORGANIZATION REPORT NUMBER(S)
AMI Report 8706

5 MONITORING ORGANIZATION REPORT NUMBER(S)
AFOSR-TR- 87-1418

6a. NAME OF PERFORMING ORGANIZATION
Analytical Methods, Inc.

6b. OFFICE SYMBOL (If applicable)

7a NAME OF MONITORING ORGANIZATION
Air Force Office of Scientific Research

6c. ADDRESS (City, State and ZIP Code)
2133 - 152nd Avenue N.E.
Redmond, WA 98052

7b. ADDRESS (City, State and ZIP Code)
Building 410
Bolling AFB, D.C. 20332

8a. NAME OF FUNDING/SPONSORING ORGANIZATION
AFOSR/NA
Bolling AFB, DC 20332

8b. OFFICE SYMBOL (If applicable)
AFOSR/NA

9. PROCUREMENT INSTRUMENT IDENTIFICATION NUMBER
F49620-84-C-0033

8c. ADDRESS (City, State and ZIP Code)
AFOSR/NA/Bldg 410
Bolling AFB, DC 20332

10. SOURCE OF FUNDING NOS.

PROGRAM ELEMENT NO.	PROJECT NO.	TASK NO.	WORK UNIT NO.
61102F	2307	A2	

11. TITLE (Include Security Classification)
PREDICTING DYNAMIC SEPARATION CHARACTERISTICS OF GENERAL CONFIGURATIONS (Unclassified)

12. PERSONAL AUTHOR(S)
Maskew, Brian

13a. TYPE OF REPORT	13b. TIME COVERED	14. DATE OF REPORT (Yr., Mo., Day)	15. PAGE COUNT
FINAL	FROM 4/84 TO 7/87	7/28/87	43

16. SUPPLEMENTARY NOTATION

17. COSATI CODES		
FIELD	GROUP	SUB. GR

18. SUBJECT TERMS (Continue on reverse if necessary and identify by block number)
UNSTEADY; TIME-STEPPING CALCULATIONS;
DYNAMIC SEPARATED WAKE MODEL;
COUPLED VISCOUS/INVISCID CALCULATION,

19. ABSTRACT (Continue on reverse if necessary and identify by block number)

A procedure has been developed for treating the dynamic interaction between a separated wake and a surface undergoing an unsteady motion. The basis of the method is an unsteady (time-stepping) panel method coupled with unsteady integral boundary layer codes. Pilot codes have been developed for both two- and three-dimensional conditions. Results presented here are mainly from the two-dimensional code in which the various routines for controlling the dynamic wake model have been developed. Some viscous/inviscid three-dimensional results are shown. The long term objective is to treat complete aircraft configurations through high angle-of-attack maneuvers.

DTIC ELECTE OCT 26 1987 D

20. DISTRIBUTION/AVAILABILITY OF ABSTRACT
UNCLASSIFIED/UNLIMITED ☒ SAME AS RPT ☐ DTIC USERS ☐

21. ABSTRACT SECURITY CLASSIFICATION
UNCLASSIFIED

22a. NAME OF RESPONSIBLE INDIVIDUAL	22b TELEPHONE NUMBER (Include Area Code)	22c. OFFICE SYMBOL
Capt. Hank E. Helin	(202) 767-4935	AFOSR/NA

DD FORM 1473, 83 APR EDITION OF 1 JAN 73 IS OBSOLETE

UNCLASSIFIED
SECURITY CLASSIFICATION OF THIS PAGE

87 10 13 078

Analytical Methods Report 8706

FINAL REPORT

AFOSR-TR- 87-1418

PREDICTING DYNAMIC SEPARATION CHARACTERISTICS OF GENERAL CONFIGURATIONS

B. Maskew and F.A. Dvorak

Prepared under Contract F49620-82-C-0033

DTIC

Submitted to:

AFOSR/NA
Bolling Air Force Base
Washington, D.C. 20332

sion For
NTIS GRA&I
DTIC TAB
Unannounced
Justification
Distribution/
Availability Codes
Dist Special
A-1

Submitted by:

Analytical Methods, Inc.
2133 - 152nd Avenue N.E.
Redmond, Washington 98052
(206) 643-9090

July 1987

TABLE OF CONTENTS

		Page
ABSTRACT		1
1.0	INTRODUCTION	2
2.0	METHOD FORMULATION	4
3.0	NUMERICAL PROCEDURE	8
	3.1 Initial Setup	8
	3.2 Geometry Definition	8
	3.3 Matrix of Influence Coefficients	8
	3.4 Potential Flow Solution	11
	3.5 Boundary Layer Analysis	12
	3.6 Wake Routines	12
4.0	RESULTS	15
5.0	CONCLUSIONS	40
6.0	REFERENCES	41

LIST OF FIGURES

Fig. No.	Title	Page
1	Features of the Simplified Flow Model	5
2	Aircraft Movement Relative to the Inertial Frame	7
3	Outline of the Numerical Procedure	9
4	Geometry Reference Frame	10
5	Wake Movement Viewed in the Aircraft Frame . . .	13
6	Indicial Lift and Circulation for an Impulsively Started Airfoil	16
7	Effect of Time-Step Size on Calculated Indicial Lift for an Impulsively Started NACA 0012	17
8	Comparison of Real and Imaginary Lifts as a Function of Reduced Frequency	18
9	Calculated C_L ~ Time for a NACA 0012 Oscillating in Pitch about the Quarter Chord	19
10(a)	Calculated Drag History for a 60° Wedge Started Impulsively from Rest	20
(b)	Calculated Pressure Distribution for a 60° Wedge Started Impulsively from Rest	21
11	Calculated Drag Coefficient of Two-Dimensional Wedges as a Function of Semi-Apex Angle	23
12	Airfoil with Spoiler Deflected 30°	
(a)	Samples from Computed Wake Development	24
(b)	Base Pressure behind Spoiler	25
(c)	Lift Coefficient	25
13	Comparison of Calculated and Measured Lift on a NACA 0012 Airfoil Oscillating in Pitch about the Quarter Chord	26
14(a)	NACA 0012 Starting Impulsively from Rest Pitching from 10° to 30°; $\dot{\alpha}c/2U_\infty = 0.175$	28

LIST OF FIGURES (CONCLUDED)

Fig. No.	Title	Page
14(b)	(i) NACA 0012 Starting Impulsively from Rest Pitching from 10° to 30°; $\dot{\alpha}c/2U_\infty$ = 0.175; τ = 0.6	29
	(ii) NACA 0012 Starting Impulsively from Rest Pitching from 10° to 30°; $\dot{\alpha}c/2U_\infty$ = 0.175, τ = 1.6	30
15	Comparison of Calculated and Measured Lift and Pressure Drag on a NACA 0012 Section During Pitch-up Motion about s/c = .317	
(a)	k = 0.047, α_{max} = 60°	31
(b)	k = 0.089, α_{max} = 56°	32
(c)	k = 0.13, α_{max} = 55°	33
16	Comparison with the Pitch-up Data of Helin and Walker (20)	
(a)	Wake Geometry at Two Time STeps	35
(b)	Variation of Velocity at s/c = 0.7 Versus Angle of Attack	36
17(a)	Comparison of Chordwise Pressure Distribution (Real Part) at y/s = 0.70 between Computed and DFVLR Data	37
(b)	Comparison of Chordwise Pressure Distribution (Imaginary Part) at y/s = 0.70 between Computed and DFVLR Data	38
(c)	Comparison of Chordwise Pressure Distribution between Computed and DFVLR Data (α_o = 12°, α_i = 1.07, k = .3, Rn = 1.35 x 10^6, Spanwise Location, η = 0.7	39

ABSTRACT

A procedure has been developed for treating the dynamic interaction between a separated wake and a surface undergoing an unsteady motion. The basis of the method is an unsteady (time-stepping) panel method coupled with unsteady integral boundary layer codes. Pilot codes have been developed for both two- and three-dimensional conditions. Results presented here are mainly from the two-dimensional code in which the various routines for controlling the dynamic wake model have been developed. Some viscous/inviscid three-dimensional results are shown. The long term objective is to treat complete aircraft configurations through high angle-of-attack maneuvers.

1.0 INTRODUCTION

Recent interest in the concept of supermaneuverability (e.g., (1) and (2)) has stimulated renewed efforts to explore ways of predicting the unsteady flow characteristics of combat aircraft in high angle-of-attack maneuvers. The problem requires treatment of general configurations having separated flows whose extent varies with time and whose downstream development culminates in complex, energetic vortical structures which strongly interact with the aircraft surfaces. It is this interaction which greatly affects the dynamic behavior of the aircraft and which needs to be understood and to be predictable if the supermaneuverable concept is to be exploited and integrated into new designs.

Strictly the above problem requires treatment by the Navier-Stokes equations, but such solutions are very expensive and are currently limited to fairly simple configurations (e.g., see the recent review by Laschka (3)). The geometric complexity of modern combat aircraft is clearly beyond practical treatment by Navier-Stokes solvers and is likely to remain so for some time to come. The present project, therefore, examines an alternative approach based on coupling between unsteady boundary layer methods and an unsteady (time-stepping) panel method which includes a dynamic wake model.

Panel codes such as VSAERO (4) routinely handle the geometry of complex aircraft configurations. The calculated steady and quasi-steady aerodynamic characteristics include corrections for "real flow" effects: iteratively coupled boundary layer codes and a wake relaxation routine modify the basic inviscid solution and the effects of compressibility are treated by approximate corrections such as those of Prandtl-Glauert or Karman-Tsien. Also, separated flow problems have been successfully treated using vortex sheet modeling of the free shear layers "enclosing" the separated regions (5). The low computing cost of the basic VSAERO method has allowed practical time-stepping calculations to be performed with fairly complex geometries (6).

The separated flow and unsteady capabilities have now been combined in a new formulation installed in both two- and three-dimensional pilot codes. These have already demonstrated a cost effective, powerful capability (7). The present approach avoids the empiricisms of many of the earlier methods for unsteady separated flows (e.g., see the reviews by McCroskey (8), (9)). It extends the unsteady capability for thin wings offered by various vortex-lattice methods, e.g., Rehbach (10), Kandil (11), and Levin and Katz (12), to the case of thick wings with fuselages, etc., comprising a complete aircraft configuration. The greater details of surface pressure and velocity distributions offered by the approach allow viscous effects to be included through coupled unsteady boundary layer methods. In this respect the present approach parallels the two-dimensional work by Strickland et al. (13) and the investigations by Geissler (14).

The long term objective of the present approach is to provide a practical engineering tool capable of treating complete aircraft configurations in arbitrary motion. While separation lines are provided by the unsteady boundary layer calculations, the approach is concerned more with the effects of the large-scale vortical structures and their dynamic interactions with the vehicle surfaces than with the small-scale details of the viscous regions. However, the method should provide a basis for future couplings with more complete treatment of the surface viscous effects of unsteady separating flows such as those being pursued by Geissler (14), Cebeci et al. (15) and Le Balleur (16), among others. In addition, the method provides a foundation for applying improved modeling techniques resulting from further evaluation of experimental results such as those of McCroskey and Philippe (17), McAlister and Carr (18), Francis, Keese and Retelle (19), Helin and Walker (20), and Graham and Strickland (21).

Finally, the approach presented here has a potential application to a broad range of unsteady problems involving arbitrary geometries and arbitrary motions.

2.0 METHOD FORMULATION

The problem is first reduced to a flow model in which the aircraft and its wake are immersed in an inviscid, irrotational and incompressible flow; regions dominated by viscous effects are assumed to be confined to the wake and to thin boundary layers on the aircraft surfaces. Furthermore, the separated wakes are assumed to be contained within thin shear layers--represented by vortex sheets. These sheets are allowed to distort and to roll up to form discrete vortices which, for numerical purposes, are given a small but finite "core". The wake fluid between the vortex sheets and external to the vortex cores is assumed to be a low-energy potential flow. Figure 1 illustrates the features of the model. It shows a section taken through a wing undergoing a high α pitch maneuver. The wake vortex sheets contain the start of vortex roll-up due to the transient in the rate of vorticity shedding. This simple model of an extensive separated region has been used successfully in the "steady" separated flow case (5), (22), and for unsteady separated flows from thin sharp-edge surfaces (12). It is justifiable based on experimental observations that the rate of vorticity dissipation in the separated free-shear layers is initially very low.

Consider the external flow; the initial assumptions above allow a velocity potential, ϕ, to be defined, and the continuity equation reduces to Laplace's equation.

$$\nabla^2\phi = 0$$

This, coupled with Green's Theorem, yields the basic equation for the panel method (e.g., see (6)). The form used here employs the internal Dirichlet boundary condition of zero perturbation potential applied at points P on the inside of the aircraft surface, S:

$$\iint_{S-P} \mu \mathbf{n} \cdot \nabla\left(\frac{1}{r}\right) dS - 2\pi\mu_P + \iint_S \frac{\sigma}{r}\, ds$$

$$+ \iint_W \mu_W \mathbf{n} \cdot \nabla\left(\frac{1}{r}\right) dW = 0 \qquad (1)$$

where S-P signifies that the integral excludes the point, P, whose contribution is given by the second term. $\mathbf{n}$ is the unit normal to the surface, S, or to the wake, W; r is the distance form an inducing element, dS or dW, to the point P; μ is the surface perturbation potential divided by 4π; and μ_W is the jump in total potential across the wake sheet divided by 4π. σ, the source strength, is equal to the normal component of the perturbation velocity, v, divided by 4π; i.e.,

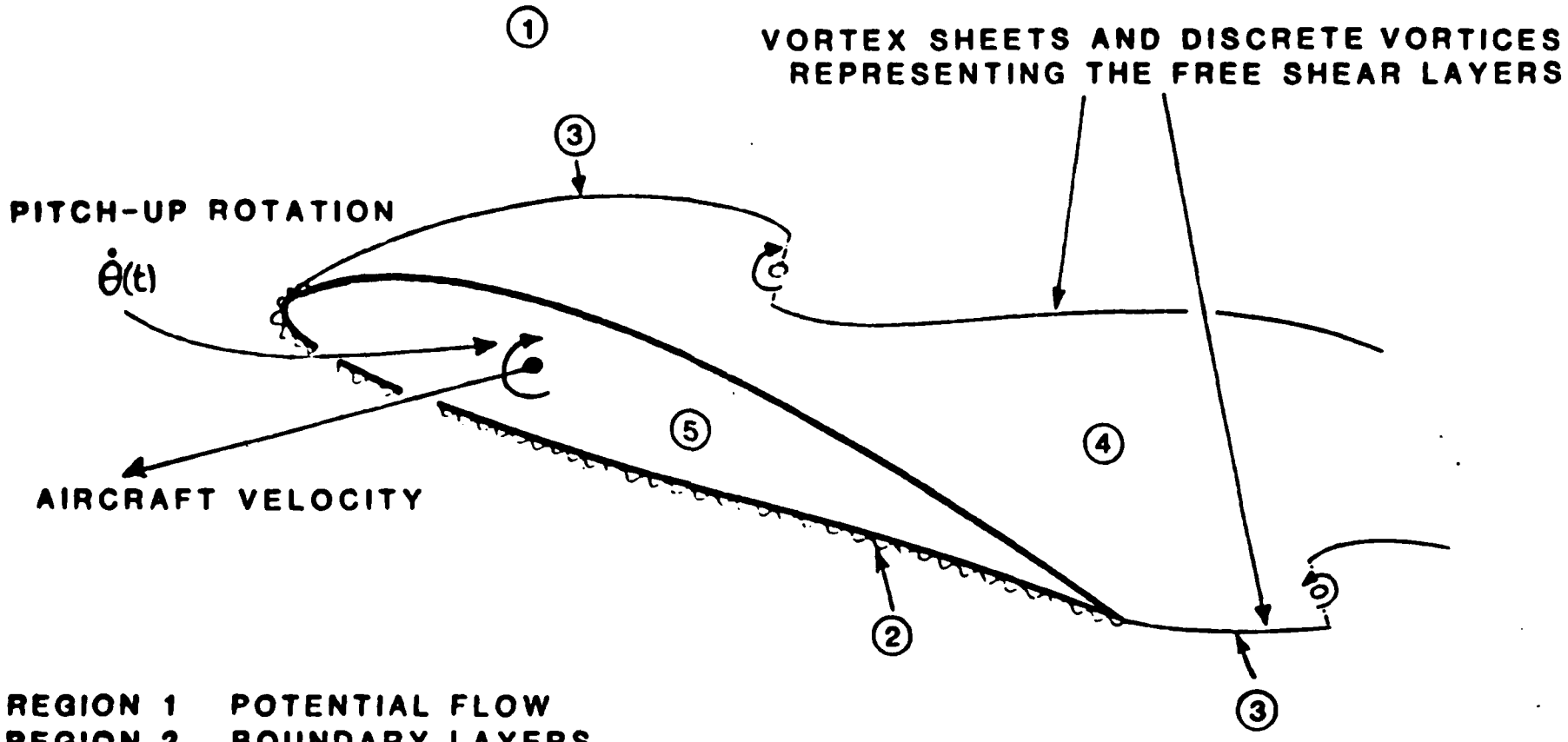

REGION 1 POTENTIAL FLOW
REGION 2 BOUNDARY LAYERS
REGION 3 FREE SHEAR LAYERS
REGION 4 POTENTIAL FLOW (LOW ENERGY)
REGION 5 POTENTIAL FLOW (FICTITIOUS INTERNAL FLOW)

Figure 1. Features of the Simplified Flow Model.

$$\sigma = \mathbf{n} \cdot \mathbf{v}/4\pi \tag{2}$$

It is observed from Eq. (1) that in the present formulation the wake is represented by doublet singularities only (the gradient of which gives the velocity jump across the wake sheet and, hence, the local vorticity vector) and the aircraft surface is represented by doublet and source singularities. The basic unknown is the surface doublet distribution. The source distribution can be evaluated directly from the external Neuman boundary condition applied at each instant of time as described below.

The aircraft-fixed reference frame (x,y,z) is moving and rotating relative to an inertial frame (X,Y,Z), Figure 2.

The flow velocity relative to the aircraft-fixed frame is

$$\mathbf{V} = \mathbf{v} - \mathbf{V}_A - \Omega \mathbf{h} \wedge \mathbf{r} \tag{3}$$

where $\mathbf{V}_A$ is the aircraft frame velocity viewed from the inertial frame. Ω is the angular velocity about a unit axis, $\mathbf{h}$, passing through the aircraft frame origin, and $\mathbf{r}$ is the position vector of the point in the aircraft reference frame where the velocity is being evaluated.

The normal component of $\mathbf{V}$ at a point on the surface is, therefore:

$$V_N = \mathbf{n} \cdot \mathbf{V}$$

$$= \mathbf{n} \cdot \mathbf{v} - \mathbf{n} \cdot \mathbf{V}_A - \Omega \mathbf{n} \cdot \mathbf{h} \wedge \mathbf{r}$$

and using Eq. (2), the source value becomes

$$\sigma = \frac{1}{4\pi} \left| V_N + \mathbf{n} \cdot \mathbf{V}_A + \Omega \mathbf{n} \cdot \mathbf{h} \wedge \mathbf{r} \right| \tag{4}$$

The resultant normal flow velocity, V_N, relative to the aircraft surface is generally zero. However, V_N can take nonzero values to represent regions of outflow ($V_N > 0$) or regions of inflow ($V_N < 0$) to model exhaust and inlet flows, respectively; or to represent boundary layer displacement effects; i.e.,

$$V_N = \partial/\partial s \ (V_e \delta^*)$$

where V_e, δ^* are the local external velocity magnitude and boundary layer displacement thickness, respectively. The derivative is taken with respect to distance, s, along the external streamline. The surface distribution of V_N is provided by the boundary layer calculation in the previous time step.

When a doublet solution has been obtained, velocities are calculated at points on the wake vortex sheets using Eq. (3), and the complete wake is convected downstream through a small time step. A new strip of wake is formed along the separation lines as described in the next section.

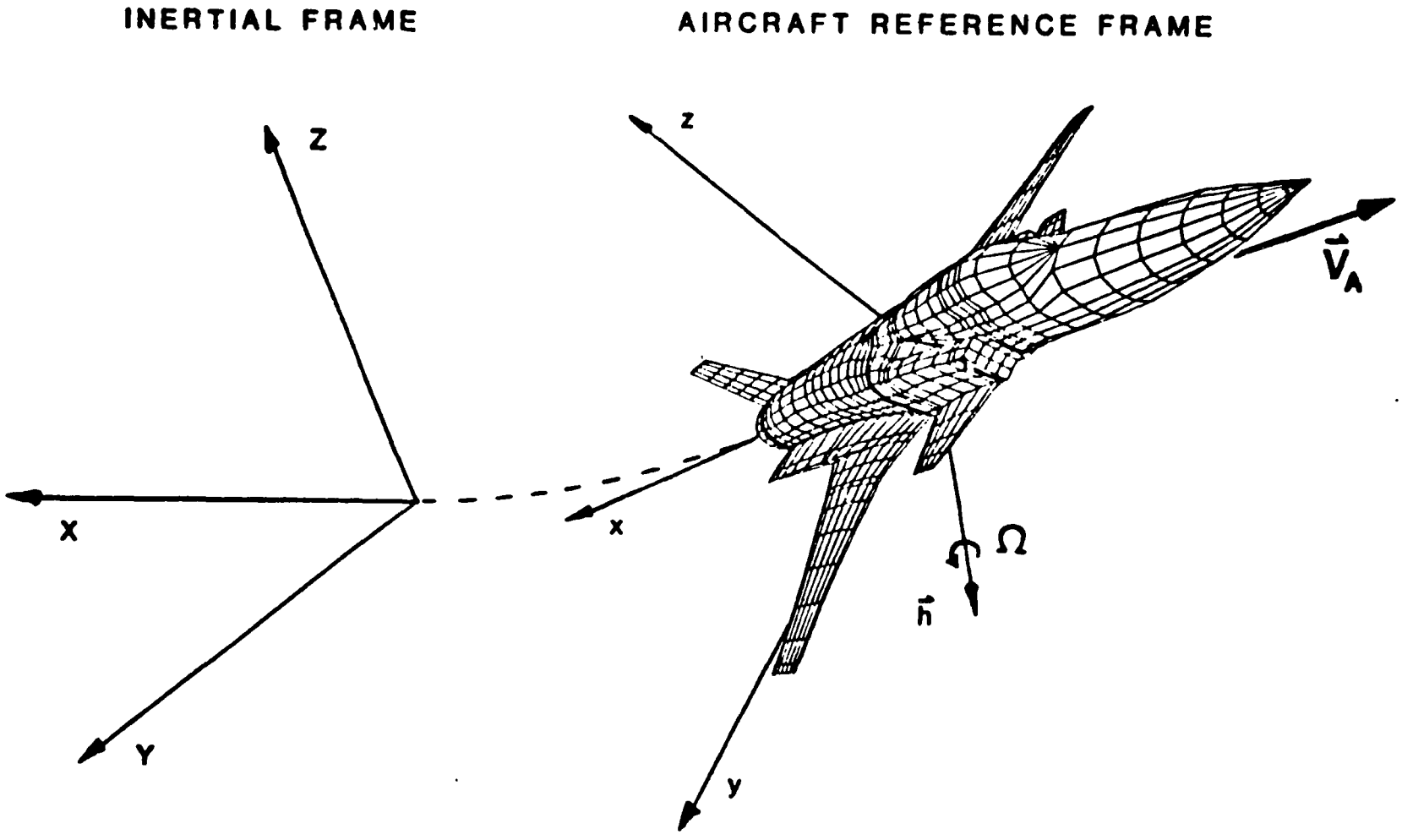

Figure 2. Aircraft Movement Relative to the Inertial Frame.

3.0 NUMERICAL PROCEDURE

The method is divided into a number of steps as shown in Figure 3. The initial setup, geometry definition and formation of the basic matrix of influence coefficients for the aircraft surface occur outside the time step loop. The calculations can start either with a wake, i.e., an initial steady-state condition, or without a wake. The latter implies an impulsive start. The calculations then proceed through the potential flow solution and boundary layer analysis. The new wake is then formed while taking a small time step. Wake influence coefficients are then calculated and combined with the basic matrix to generate the next potential flow solution. The subsequent discussion outlines these steps in more detail.

3.1 Initial Setup

The initial setup requires user input to establish the general conditions for the calculations, e.g., reference quantities, type of problems, form of output required, etc. In particular, the motion and orientation of the aircraft frame relative to the inertial frame is established here as a function of time. This is assumed to be in the form of a schedule tabulated with time. For simple motions or for completely arbitrary motions, the schedule can be input directly, e.g., a schedule of time and α provides a pitch motion. Tables for certain special motions, e.g., sinusoidal oscillations coning, etc. may be generated by a subroutine given certain key parameters. Inside the program the time derivatives are evaluated using central differencing in the table.

3.2 Geometry Definition

The geometry of the aircraft is specified next. This is described within a geometry reference frame, Figure 4, which is selected by the user for convenience. This is a body-fixed frame and may be parallel to but shifted from the aircraft frame which normally has its origin at the center of gravity. The user supplies the transformation (usually x_{CG}) to move from the geometry frame to the aircraft frame.

Once the surface geometry is defined, the program generates the quadrilateral panels which represent the aircraft surface.

3.3 Matrix of Influence Coefficients

Each surface panel is assumed to have a uniform source and doublet distribution. The integrals in Eq. (1) can then be evaluated in closed form for each panel. A control point where Eq. (1) is applied is located under the center of each panel. If there are N panels representing the aircraft surface, Eq. (1) becomes

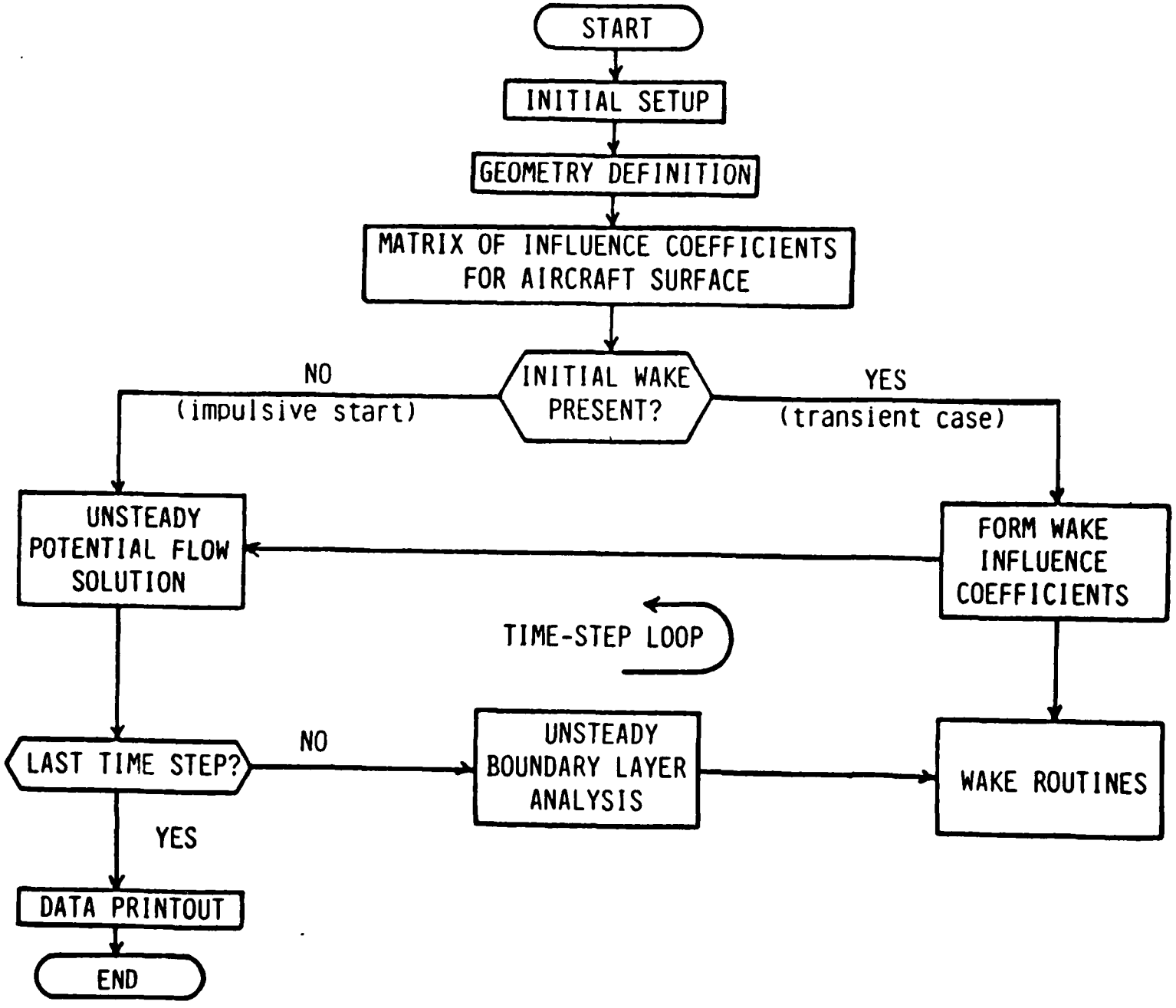

Figure 3. Outline of the Numerical Procedure.

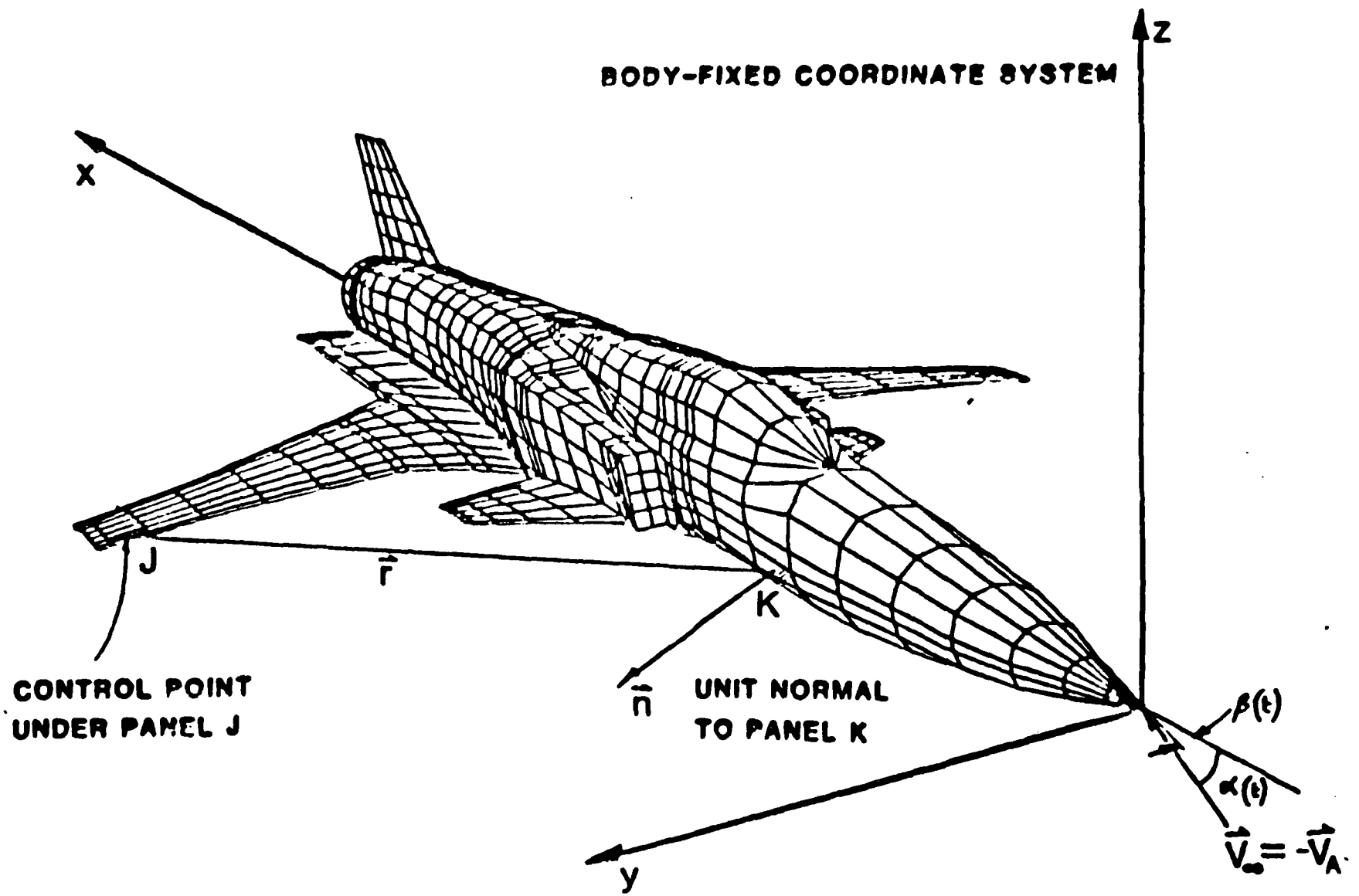

Figure 4. Geometry Reference Frame.

$$\sum_{\substack{K=1 \\ K \neq J}}^{N} \left| \mu_K C_{JK} \right| - 2\pi \mu + E_J = 0;$$

$$J = 1, \ldots N \qquad (5)$$

where μ_K is the doublet value of panel k and

$$E_J = \sum_{K=1}^{N_W} \left| \mu_{W_K} C_{JK} + \gamma_{W_K} D_{JK} \right| + \sum_{K=1}^{N} \sigma_K B_{JK}$$

N_W is the number of wake panels at this step. C_{JK}, B_{JK} are the influence coefficients for unit doublet and source uniform distributions on a quadrilateral panel. σ_K is the instantaneous panel source value from Eq. (4). This is regarded in several parts for convenience in the coding.

Wake panels have a constant doublet distribution in the normal to streamwise direction and a linear doublet distribution (i.e., constant vorticity) in the streamwise direction. Hence, the wake integral term in the quantity, E_J, in Eq. (5) has an additional part: γ_{W_K} is the vorticity value on the K^{th} wake panel and D_{JK} is the vorticity influence coefficient for the quadrilateral panel. The vorticity vector is normal to the local stream direction; its modulus is the local negative gradient of the doublet distribution down the center of each column of wake panels.

The doublet values on the wake panels are known from solutions at earlier time steps. Only the values along the separation lines (including trailing edges) are unknown at each time step and these are obtained from the surface doublet solution. Actually, the values are taken from the local jump in total potential between the pair of wake shedding panels to either side of the separation line.

3.4 Potential Flow Solution

The solution to Eq. (5) provides the surface doublet values. The surface velocities and pressures can then be evaluated. The incompressible pressure coefficient is

$$Cp = \left(V_S^2 - V^2 + 2 \partial \mu / \partial t \right) / V_A^2$$

where $V_S = V_A + \Omega h \wedge r$ is the instantaneous velocity of a point on the surface relative to the inertial frame and V is the modulus of the flow velocity from Eq. (3). The perturbation velocity, v, is evaluated from the gradient of μ at each panel. A local second-order fit to the panel doublet values in two directions is differentiated to obtain this.

The pressure distribution can be integrated over the aircraft surface to yield the instantaneous force and moment coefficients. These are saved in a file for the force and moment history.

Next, the surface velocity distribution is examined to locate lines of attachment (divergence) and lines of convergence (separation) in the external flow. In the three-dimensional version, surface streamlines (external to the boundary layer) are also computed. With this information sets of points and their velocities are assembled for the boundary layer analysis.

3.5 Boundary Layer Analysis

Curle's original method (23) has been modified to calculate the unsteady boundary layer development. This is achieved by solving the unsteady momentum integral equation using a Runge-Kutta method. The turbulent boundary layer method is based on the unsteady momentum integral equation as in the laminar boundary layer method. Cousteix's entrainment relationship (24) and Lyrio/Ferziger's skin friction relationship (25) are used for closure. The details of the methods are described in Ref. 7. Tests of the procedure against experimental data and against other methods show good agreement (7).

The calculation provides the boundary layer displacement effect along each of a family of instantaneous "streamlines". This is then redistributed to the surface panels in the attached flow regions. Computed information on the location of separation is assembled and passed over to the wake routines.

3.6 Wake Routines

When a separation line is first passed to the wake routines a set of wake panels is formed simply shedding the jump in total potential ($\mu + \phi_\infty$) between each pair of surface panels to either side of the separation line. At subsequent time steps all the previous wake panels are convected downstream, each corner point traveling for time, δt, along the local computed velocity vector, Figure 5. In this process a new wake panel is formed corresponding to each surface panel at the separation line as in the first step.

Several "housekeeping" routines are necessary to complete the wake model. First, the movement of the separation line is monitored from one step to the next and restricted if necessary; e.g., downstream movement is limited to the distance, δt x local

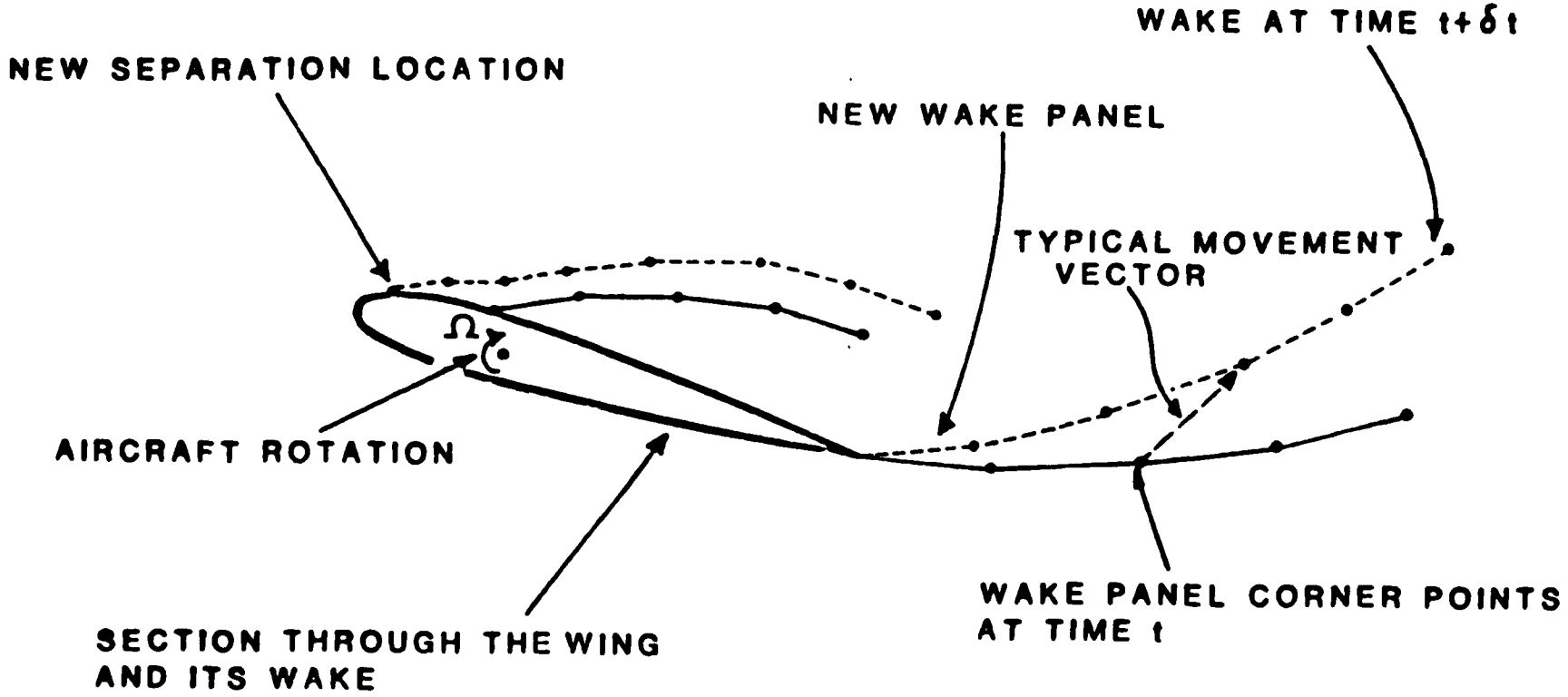

Figure 5. Wake Movement Viewed in the Aircraft Frame.

transport velocity. Also, the movement of each wake point is examined for possible impingement into the airfoil surface. This is an important routine. If an impingement is detected and if the line if impingement is at a low inclination to the panel surface, then the code simply "nudges" the point away from the surface. If the line of impingement is steep into the panel, however, then the wake is geometrically cut off at the point of intersection, usually forming a closed bubble region. Doublet values continue to be convected along this boundary in subsequent time steps, and the impingement calculation is repeated. Thus it is possible for the bubble to open again under different conditions at a later time; the wake would then proceed to grow again.

When a new wake configuration has been obtained the new wake panels and influence coefficients are formed and a new potential flow solution is computed, Figure 3.

4.0 RESULTS

As the applications increase in complexity, available test cases for comparison become scarcer. It is important, therefore, to have a set of baseline test cases of well proven results that can be checked from time to time as the method develops. Two such cases are the Wagner function for an impulsively started flat plate and the Theodorsen solution for an oscillating plate. These cases are briefly considered below to establish the accuracy of baseline solutions.

Figure 6 shows the growth of indicial lift and circulation for a NACA 0012 impulsively started from rest at an angle of attack of 0.1 rad. The curves are compared with Wagner's function for indicial lift and R.T. Jones' indicial circulation for a flat plate. The calculations, which used 31 panels around the section, are in good agreement and indicate a slightly higher trend which is consistent with a higher steady state circulation for the thickness case.

Refinements in the wake shedding model developed earlier in the two-dimensional pilot code significantly reduced the computing requirement of these time-stepping calculations. For example, Figure 7 shows the effect on indicial lift of varying the time-step size in the Wagner problem and demonstrates a rapid convergence.

The procedure has been tested also for a NACA 0012 oscillating in pitch about the quarter chord. The calculations compare favorably with the Theodorsen flat plate function over a range of reduced frequency, Figure 8. The calculations were performed with only 16 time steps per cycle. Figure 9 shows the computed results, C_L versus time, using only 4 time steps per cycle. This is in remarkably good agreement with the 16 and also 32 time-step/cycle solutions, demonstrating an extremely good convergence characteristic.

Time-stepping calculations have also been performed for cases with prescribed extensive separations. The purpose of these calculations was to check the basic unsteady circulation shedding model in the potential flow code. For the first set of tests, the wake panel were simply transported at the onset flow velocity after the initial growth as determined from the surface conditions at separation. Several triangular shapes were considered, each starting impulsively from rest and proceeding forward over 10 time steps for a total time of $\tau = \tau U_\infty / h = 3.0$, where h is the triangle base height. Separation was prescribed at the corners. Figure 10(a) shows the computed history of the drag coefficient from pressure integration for a 60 deg triangle with blunt face forward. A total of 40 panels was used to represent the triangle surface. The calculation was repeated in the presence of wind tunnel walls (also paneled) with a 10% blockage ratio. The indicated blockage correction is somewhat lower than that given by standard techniques. Figure 10(b) compares the

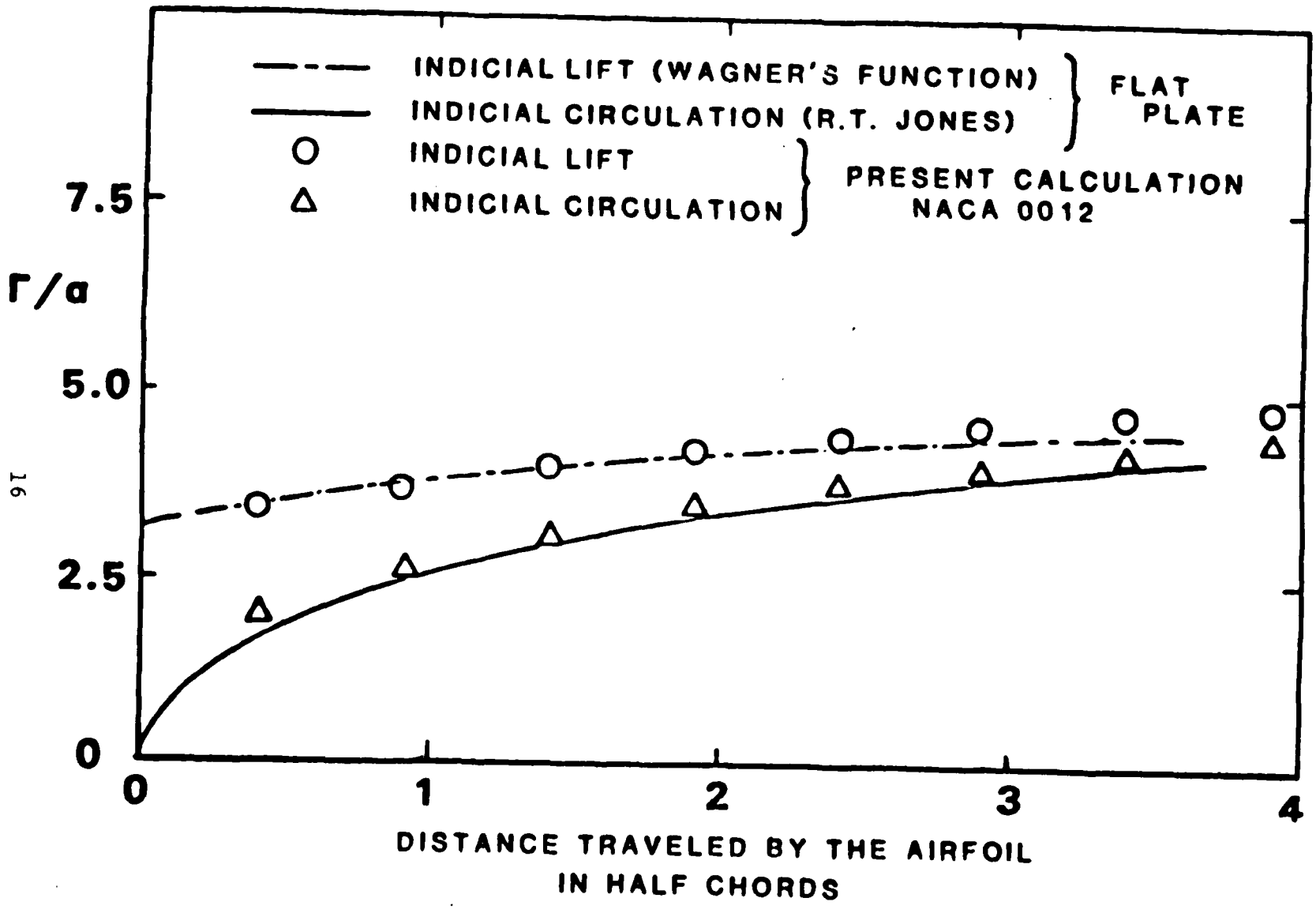

Figure 6. Indicial Lift and Circulation for an Impulsively Started Airfoil.

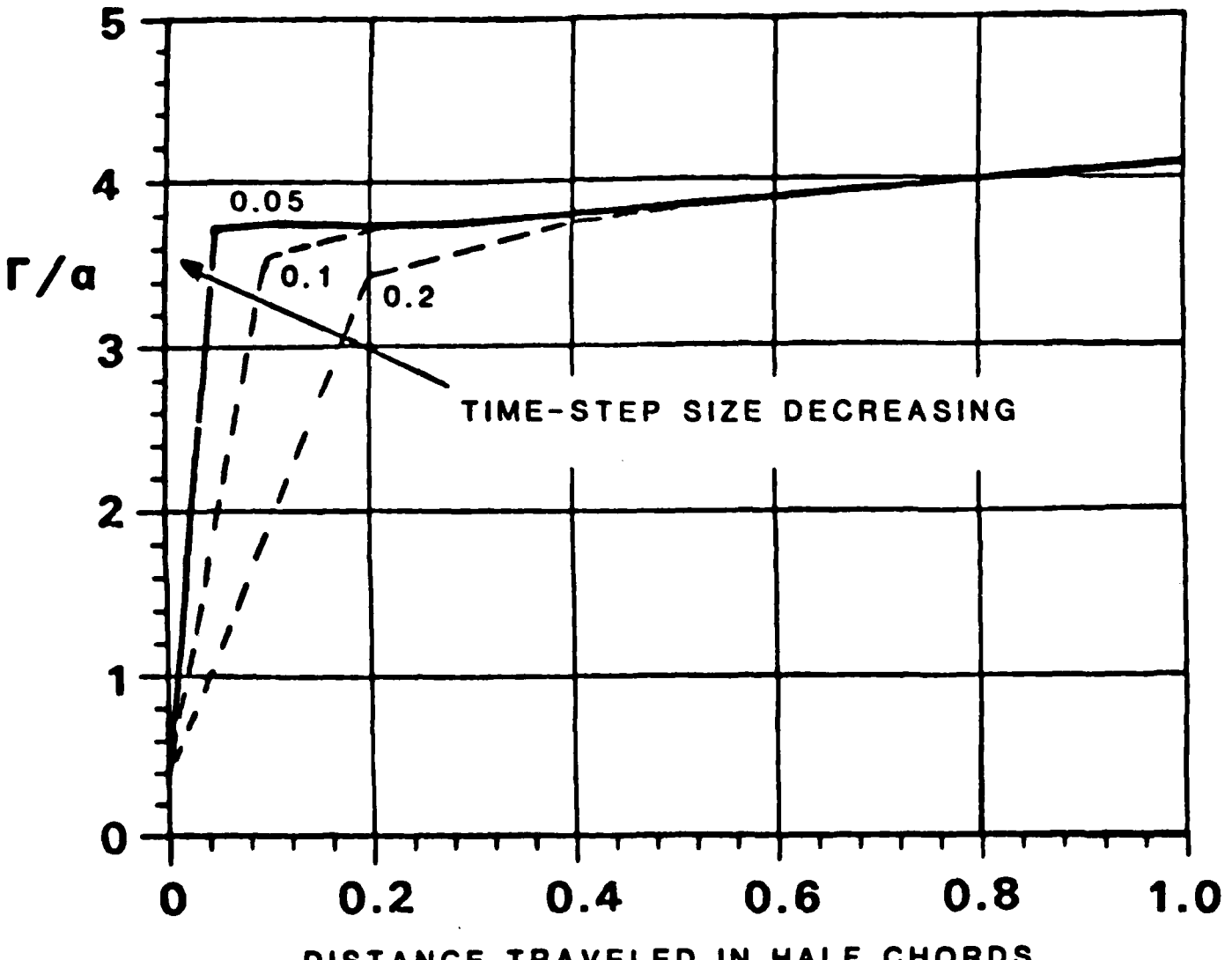

Figure 7. Effect of Time-Step Size on Calculated Indicial Lift for an Impulsively Started NACA 0012.

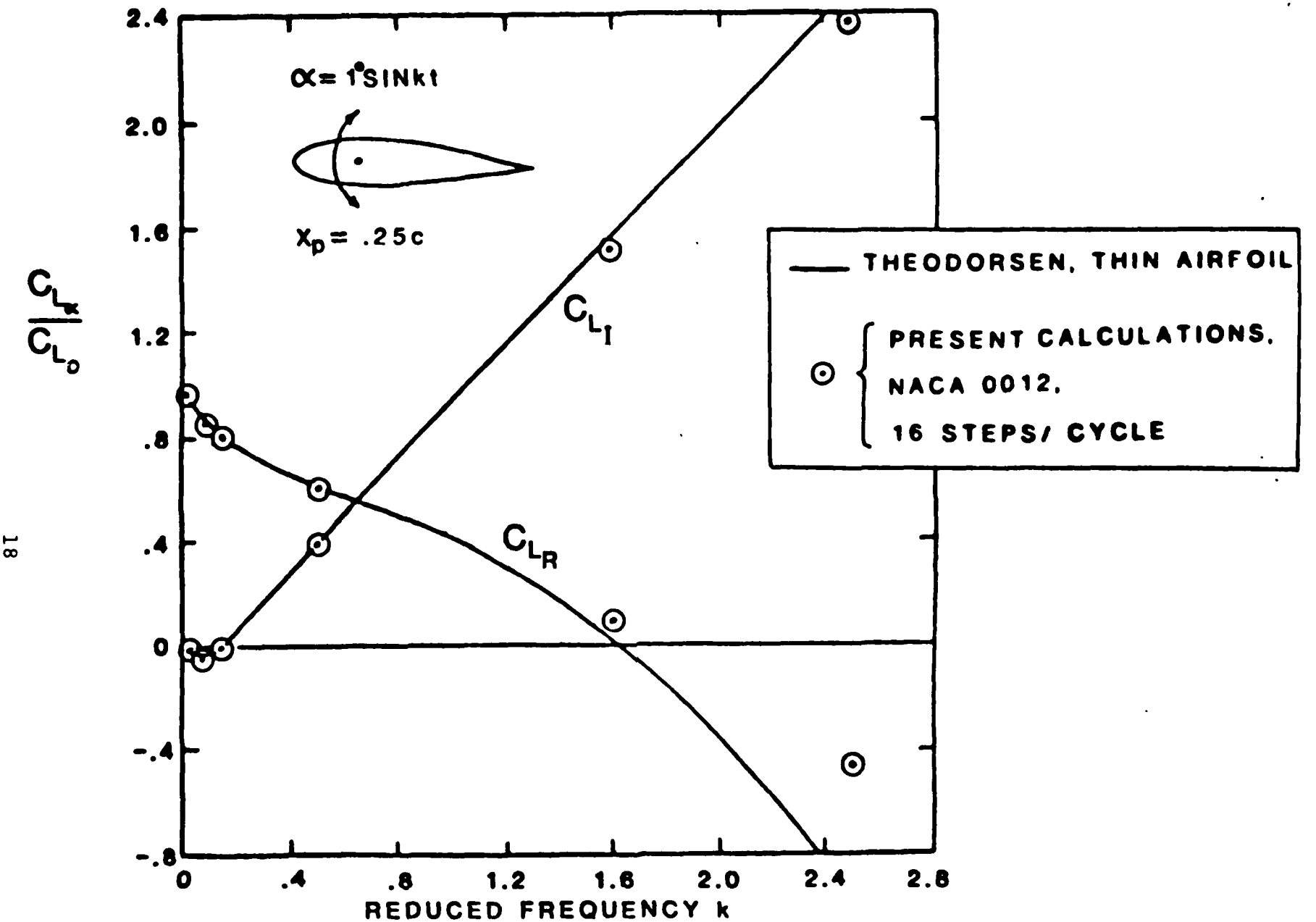

Figure 8. Comparison of Real and Imaginary Lifts as a Function of Reduced Frequency.

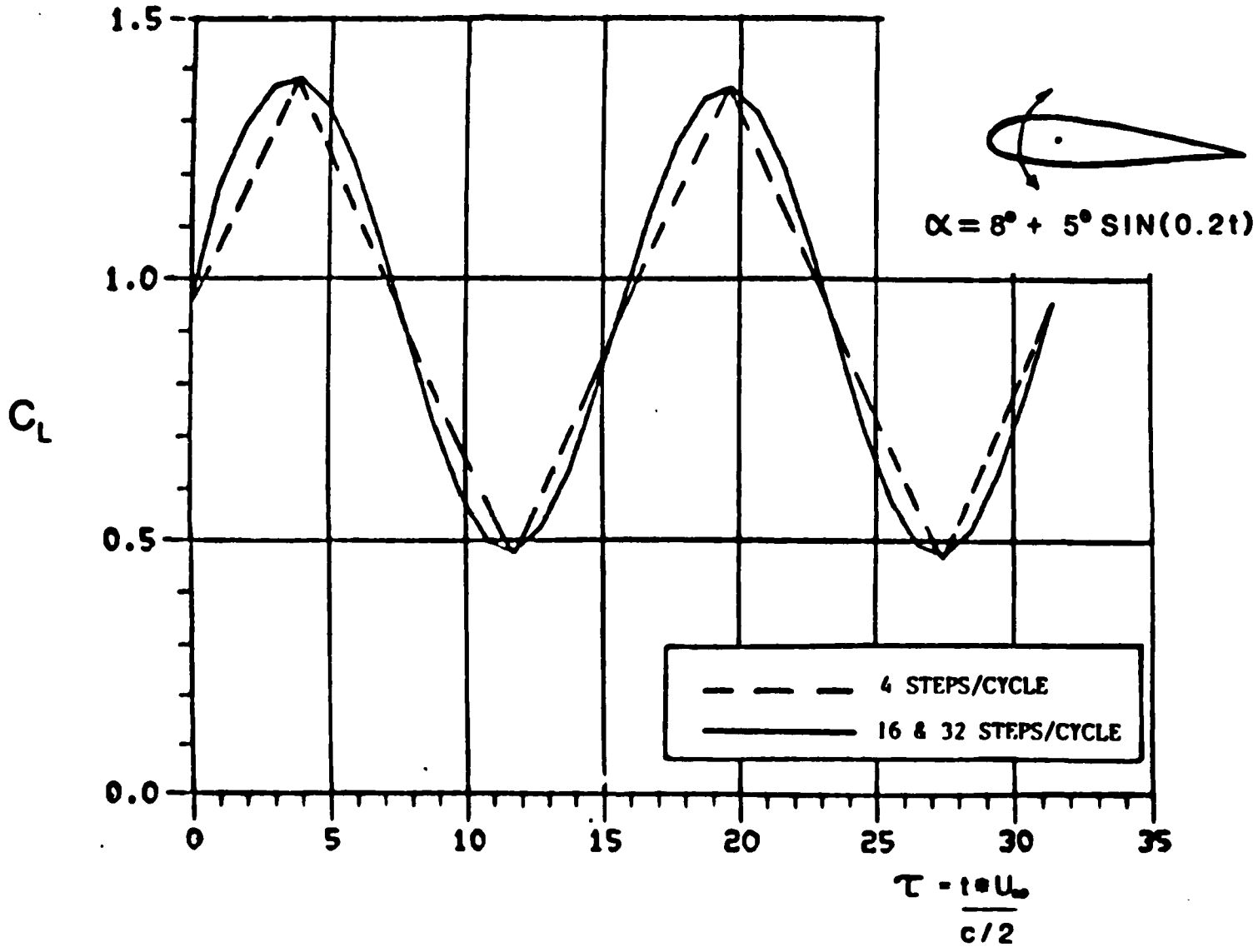

Figure 9. Calculated C_L - Time for a NACA 0012 Oscillating in Pitch about the Quarter Chord.

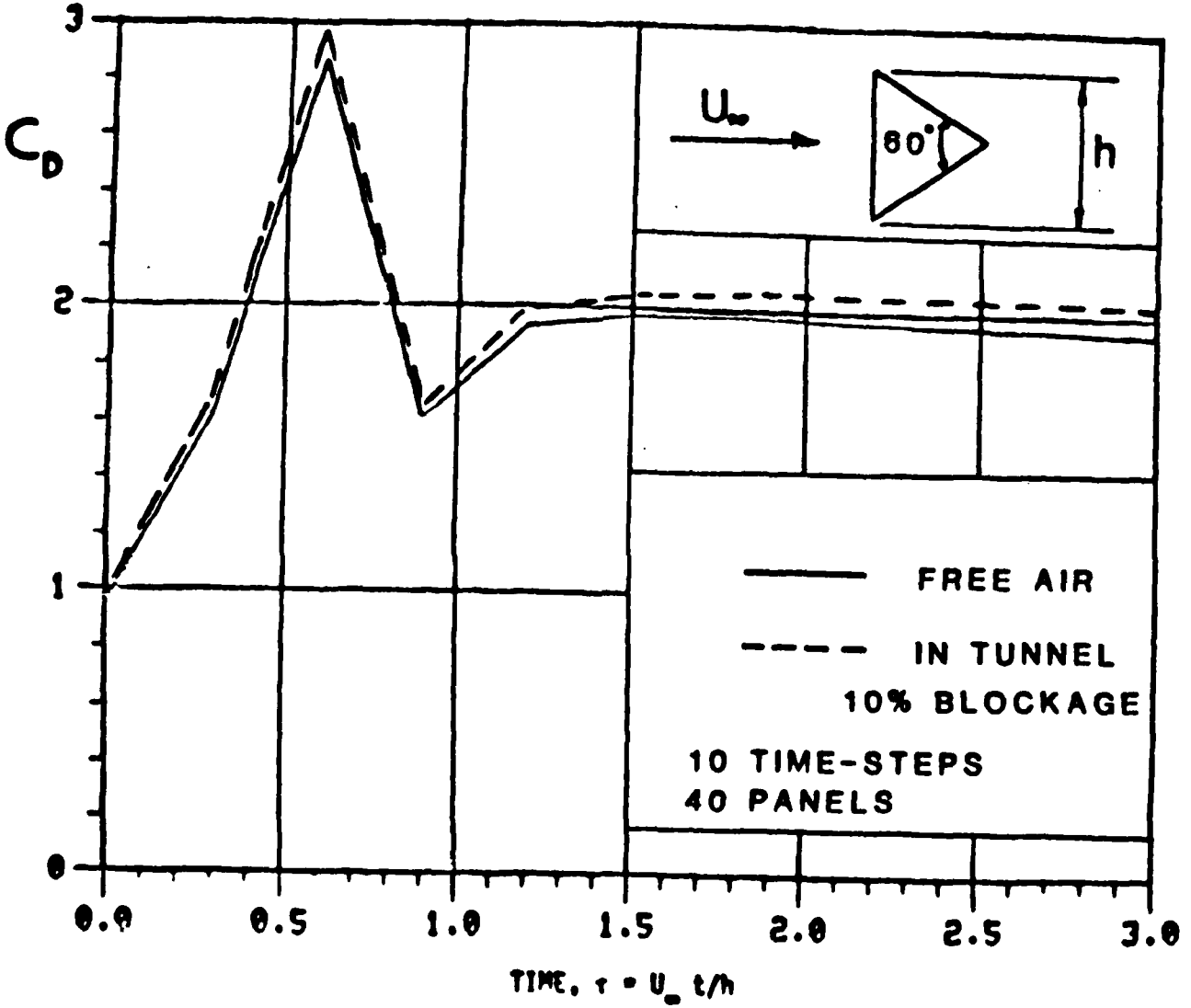

Figure 10(a). Calculated Drag History for a 60° Wedge Started Impulsively from Rest.

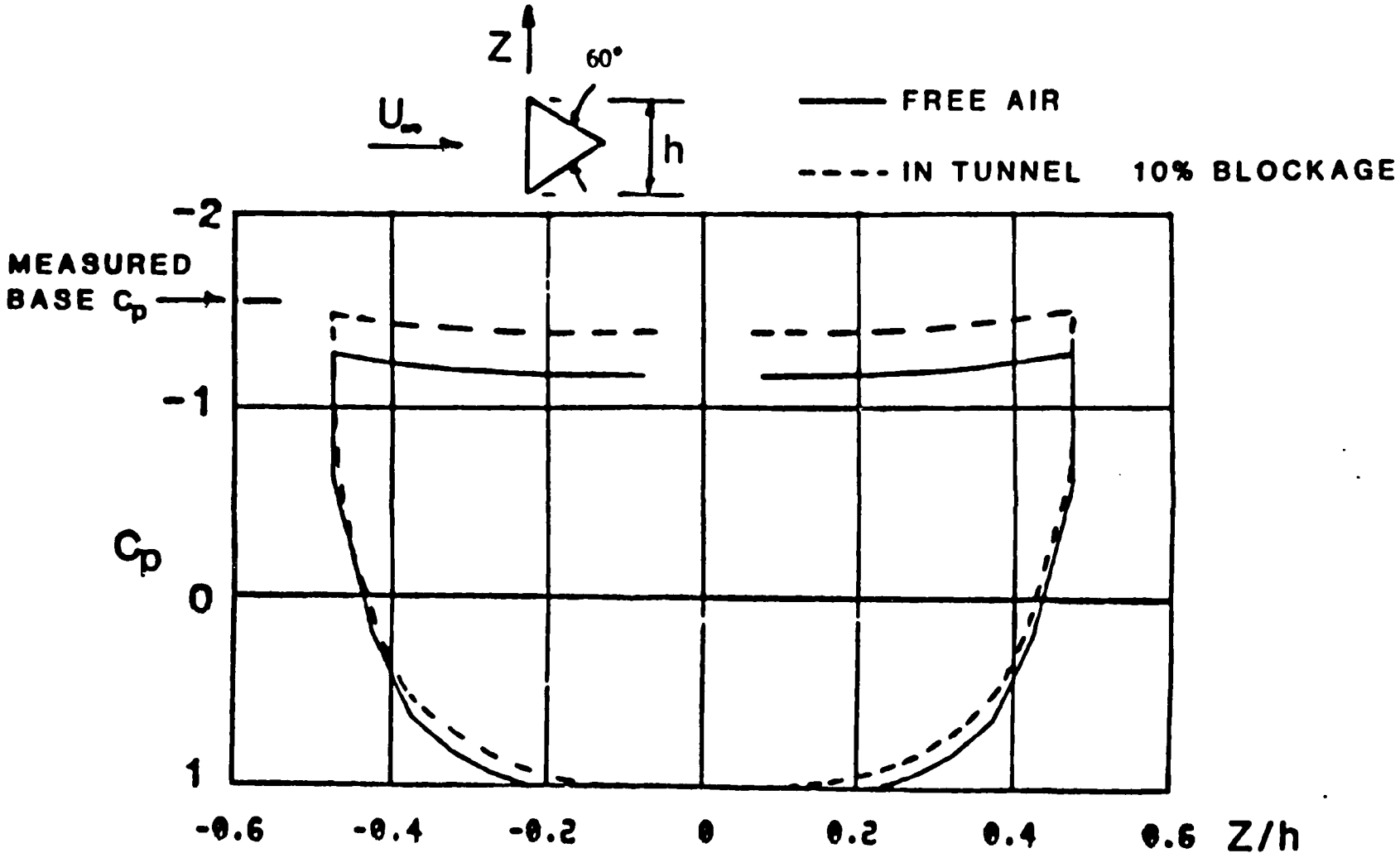

Figure 10(b). Calculated Pressure Distribution for a 60° Wedge Started Impulsively from Rest; $\tau = U_\infty t/h = 3.0$.

computed pressure distributions for this triangle in and out of the tunnel. The "base" pressure has only a small variation and is quite close to experimental measurements. Figure 11 shows a summary of computed drag coefficient versus triangle semi-apex angle. The calculated values are slightly high in relation to the experimental data collected from several sources by Hoerner (26).

One further case was run for the 60 deg, apex-forward triangle in free air with the full wake velocity calculation routine turned on but without the amalgamation and redistribution schemes at this stage. The calculated C_D for this case falls below the experimental value, Figure 11.

Although the two-dimensional pilot program was generated primarily as a tool to examine the behavior of various parts of the dynamic separation calculation, it has shown considerable promise as a general purpose code for two-dimensional calculations involving separated flows. For example, it has been applied to the cross-flow problem on helicopter booms and also to the download problems on tilt-rotor aircraft (27). Earlier examples (e.g., Figures 10 and 11) demonstrated a capability to compute base pressures and drag coefficients of blunt sections using an impulsive start. An extension of this to compute spoiler characteristics has also been briefly examined. Figure 12 shows computed wake configurations at three steps. This is for the case of a spoiler deflected 30 deg on an airfoil at α = 8 deg. The final base pressure and integrated lift, Figure 12 (b) and (c), respectively, are in good agreement with experimental measurements (28). The calculated values represent an average value over the last few time steps as the solution had started to oscillate. The amplitude on C_L is about 0.1, but the calculation ought to be continued for a longer time to examine whether a pattern between upper and lower vortex formation is established. This application could be extended further to examine pitch rates and, with a straightforward extension of the code, rates of spoiler deployment. Such an extension, involving relative motion between parts of the configuration, would also allow treatment of pitching airfoils between channel walls to assess the effects of unsteady blockage in pitch-up or oscillatory experiments.

An experimental data case for an airfoil oscillating in pitch (29) was run and the computed lift variation with α compared with the measured data in Figure 13. The airfoil is a NACA 0012 and is oscillating in pitch about the quarter-chord line with α = 8.1 deg + 4.9 deg sin (0.2t); i.e., below the dynamic stall onset. Reynolds number was 4×10^6. This reduced frequency condition is very close to the changeover from a lead to a lag situation and so there is only a small difference between the upswing and downswing curves.

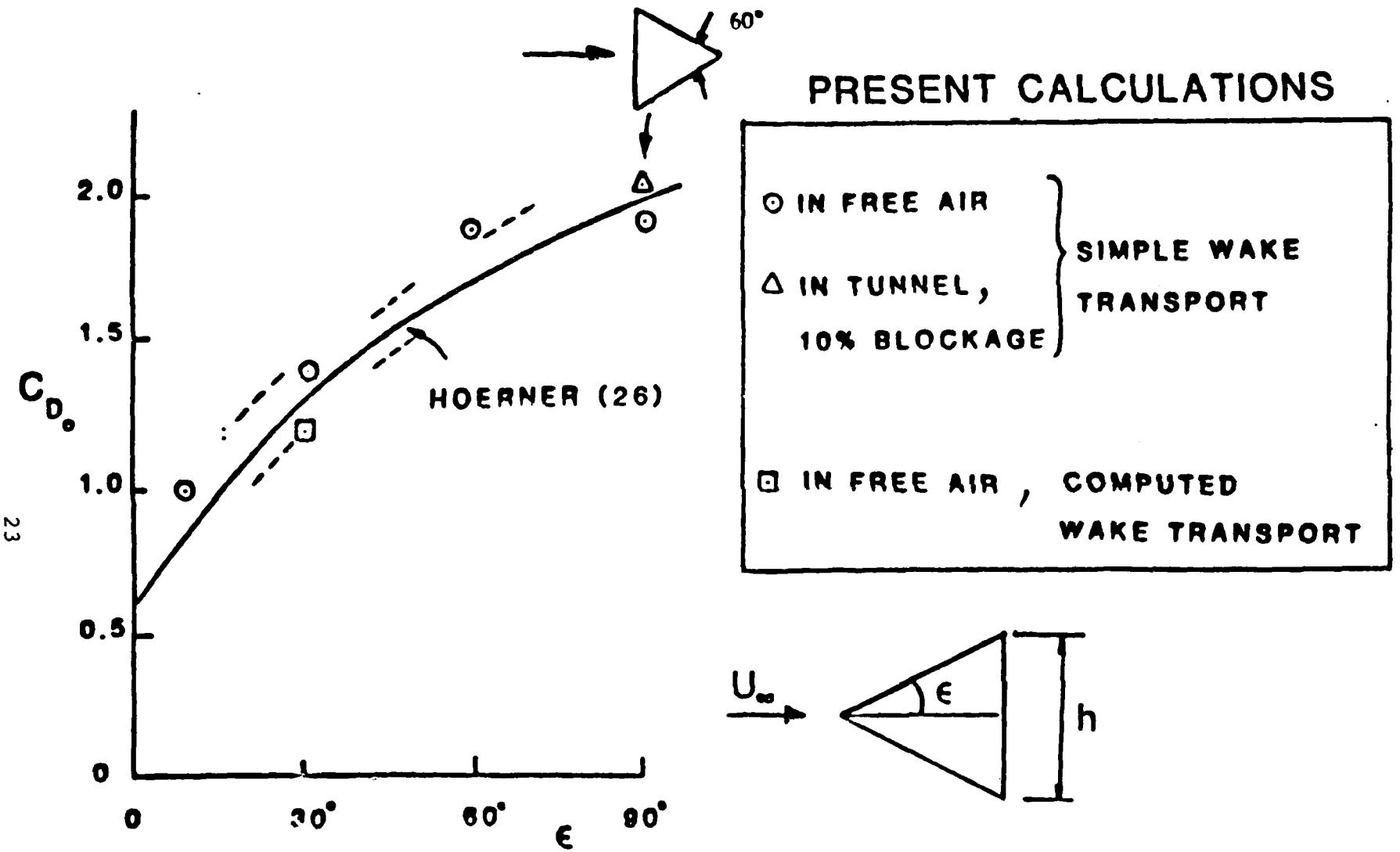

Figure 11. Calculated Drag Coefficient of Two-Dimensional Wedges as a Function of Semi-Apex Angle.

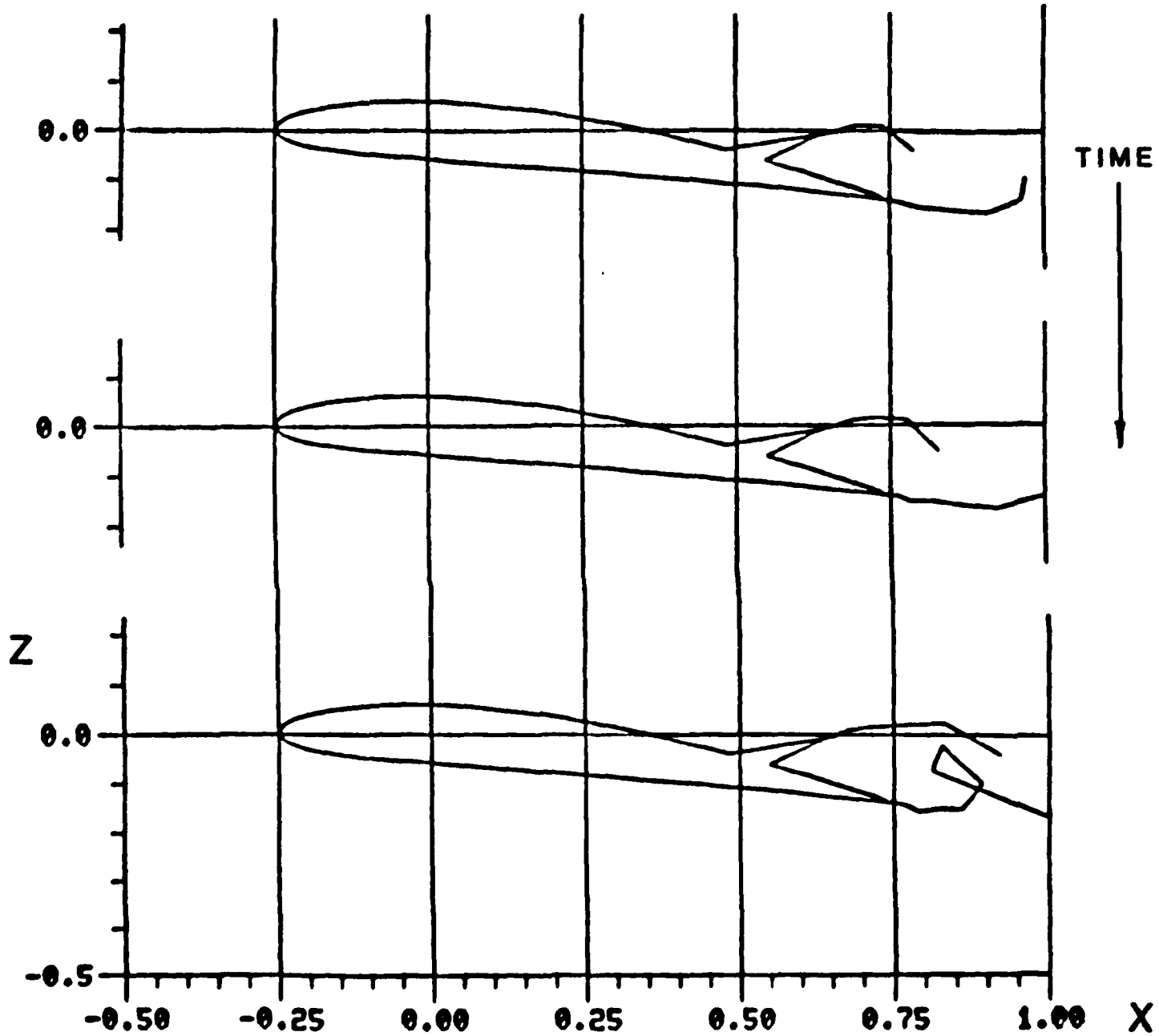

(a) Samples from Computed Wake Development

Figure 12. Airfoil with Spoiler Deflected 30°.

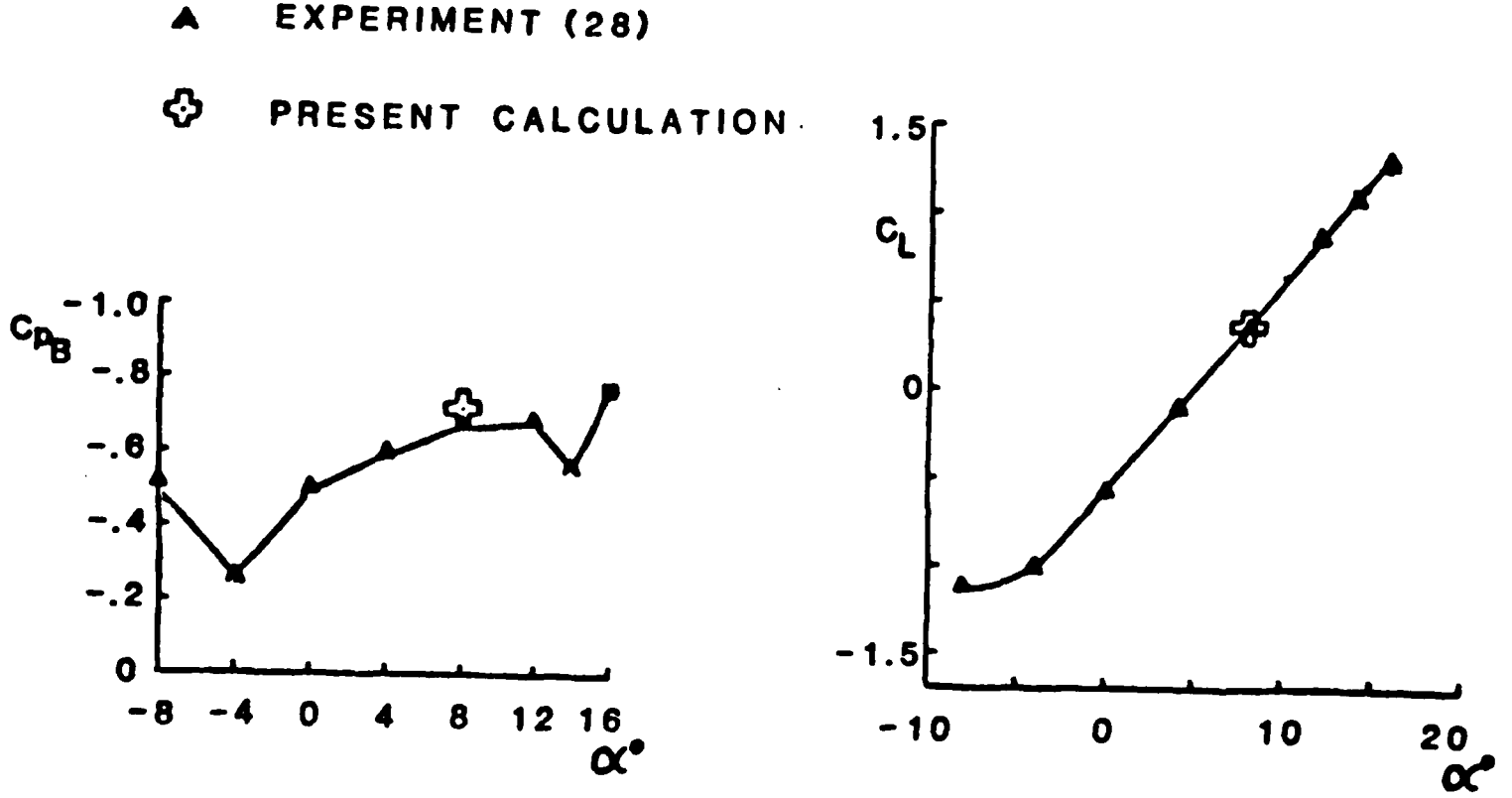

(b) Base Pressure behind Spoiler

(c) Lift Coefficient

Figure 12. Concluded.

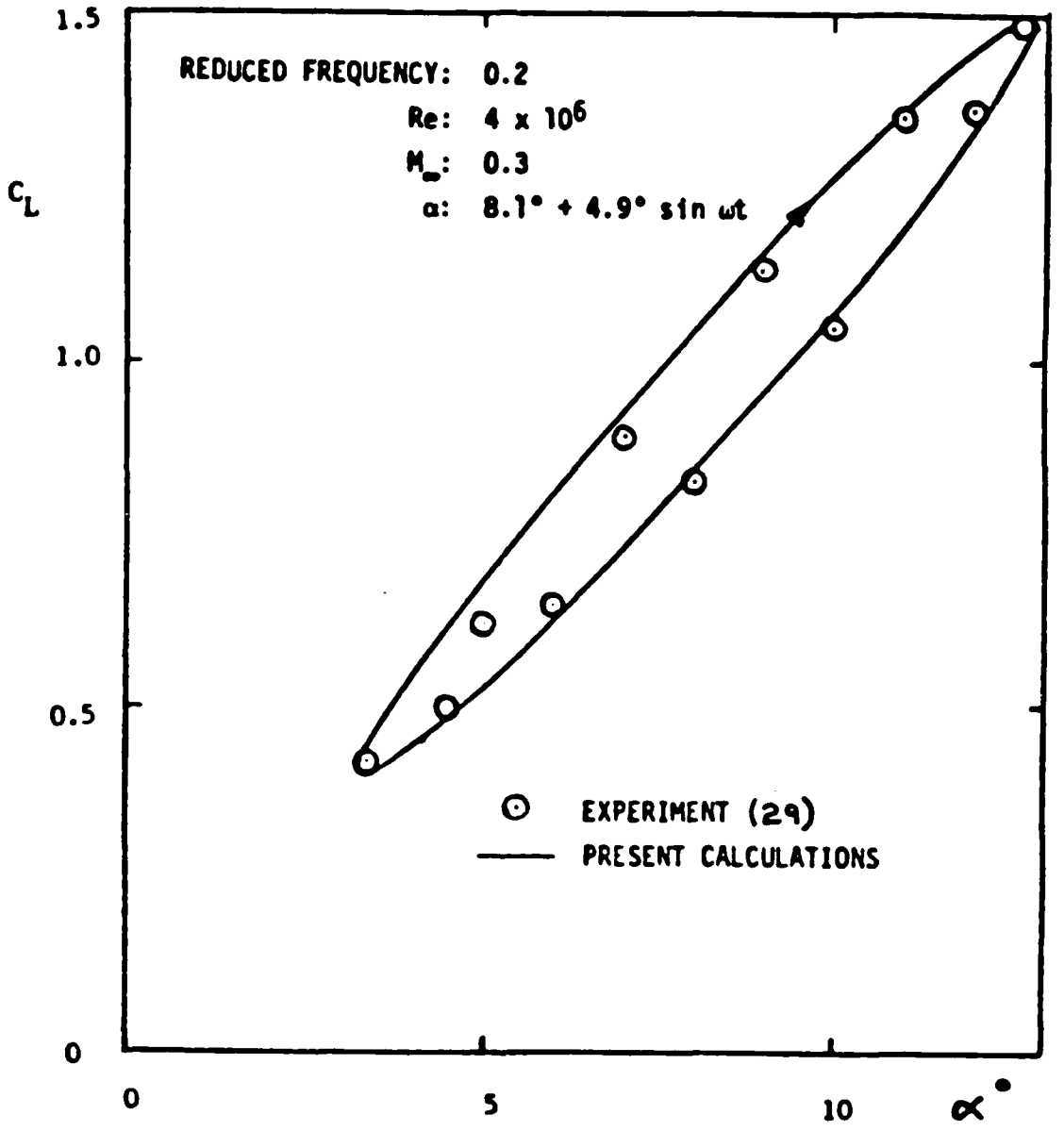

Figure 13. Comparison of Calculated and Measured Lift on a NACA 0012 Airfoil Oscillating in Pitch about the Quarter Chord.

A test calculation was performed for a NACA 0012 section in a state of pitch-up from 10 deg to 30 deg at a rate, $\dot{\alpha}c/2U_\infty$ = 0.175. The surface was represented by 30 panels. Separation point movement on the upper surface was prescribed based on boundary layer calculations performed on the pitching case with just the trailing-edge wake. (This case was run prior to the automatic coupling between the viscous and inviscid codes.) The motion was started impulsively from rest and proceeded through 10 time steps.

Figure 14(a) shows a sample of the computed wake shapes and demonstrates a reasonable numerical behavior. Sample pressure distributions are shown in Figure 14(b). The passage of the leading-edge vortex is clearly shown. This is associated with a local region of reversed flow, Figure 14(b)(ii). These were preliminary test calculations aimed at exploring the numerical behavior of the calculation procedure and potential flow model.

Experimental measurements of airfoils undergoing constant rate pitch-up motions have been taken at the Frank J. Seiler Research Laboratory (19). Three cases are considered briefly here for correlation purposes. In these cases the airfoil is pitched up from α = 0 to approximately 1 radian at a constant pitch rate and then held at constant angle of attack. Three pitch rates are considered with normalized pitch rates, k ($=\dot{\alpha}c/2U_\infty$) of 0.047, 0.089 and 0.133. Figures 15(a), (b) and (c), respectively, show the comparison between calculated and measured $C_L \sim \alpha$ and $C_D \sim \alpha$ characteristics for these cases. For the low pitch rate, k = 0.047, the comparison is very good up to about 30 deg, but then deteriorates. The calculated C_L remains fairly constant with α until the pitch rate drops to zero while the experimental curve falls markedly. The calculated rise in drag with α has a steady rate in the 30 deg to 60 deg range while the experimental measurements include a substantial increment above this rate peaking at about α = 40 deg. There is a good agreement between calculated and measured lift and drag value for the final "steady state" conditions at α = 60 deg.

One possible reason for the departure of the calculated lift and drag in the latter part of the pitch-up phase is the modeling of the leading-edge vortex roll-up. The amalgamation and redistribution schemes that were installed to stabilize the dynamic wake calculations were not performing in a consistent manner. The vortex core on the upper sheet, therefore, did not "condense" early enough in the amalgamation procedure; consequently, the vortex formed just downstream of the trailing edge and did not closely interact with the airfoil surface during the pitch-up phase. This tendency was still present at the higher pitch-up rates, k = 0.089 and k = 0.13, but to a lesser extent. In these cases the calculated lift and drag characteristics, Figures 15(b) and (c), respectively, are in very good agreement with experiment. The tendency for the measured lift to peak at about α = 30 deg is also shown in the calculated results. These calculations were not continued at α_{max} for a sufficient time to enable

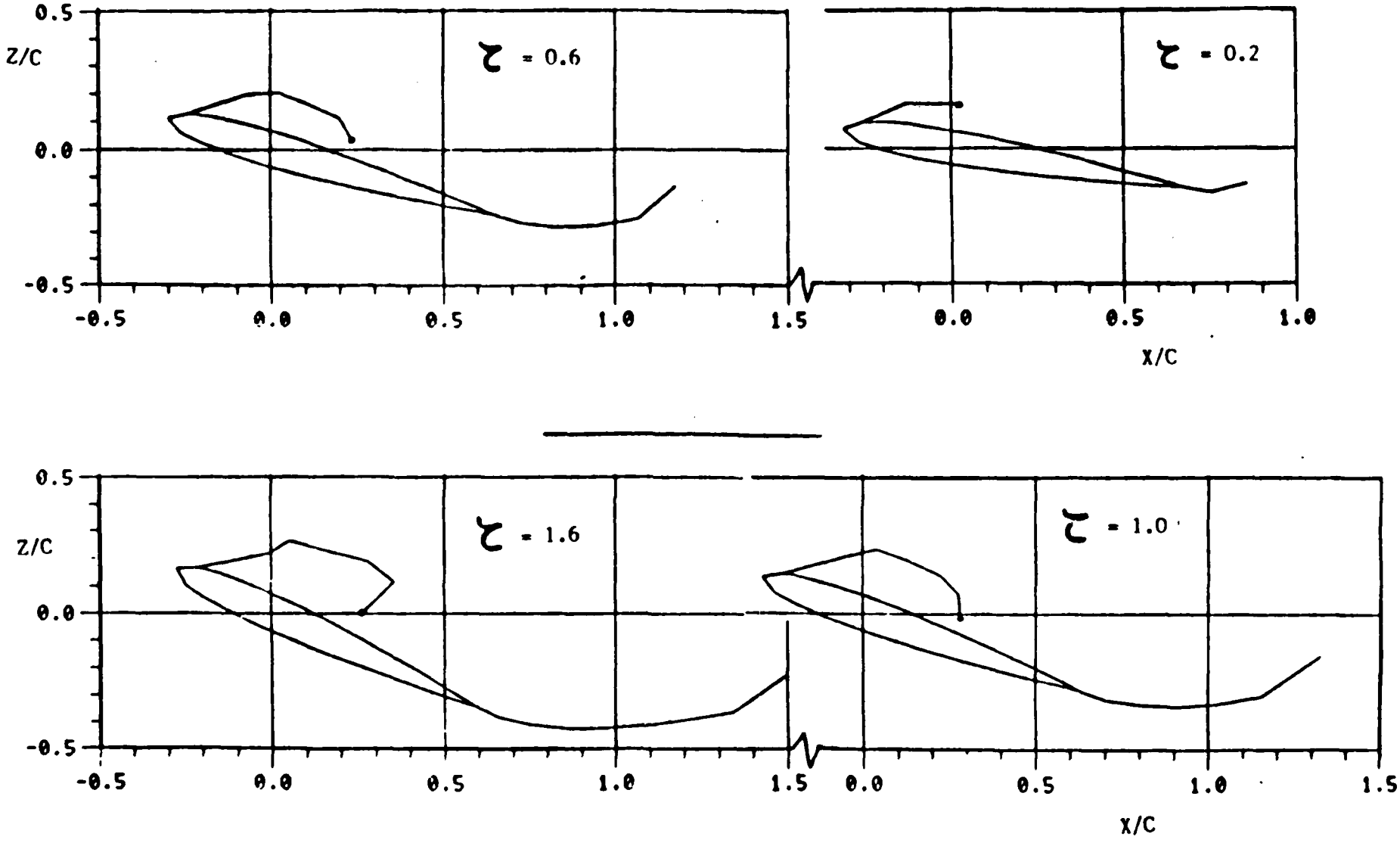

Figure 14(a). NACA 0012 Starting Impulsively from Rest Pitching from 10° to 30°: $\&c/2U_\infty = 0.175$.

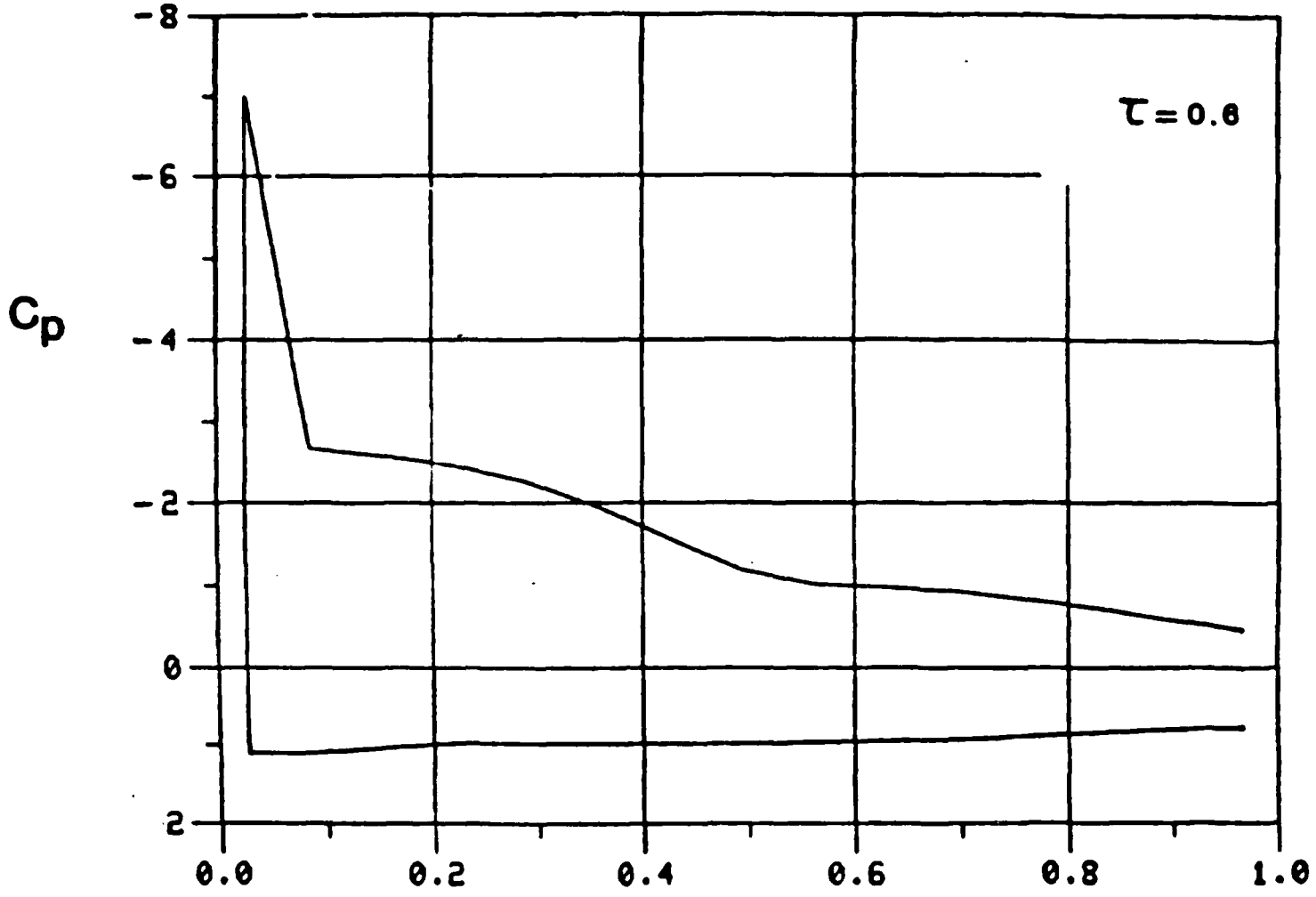

Figure 14(b)(i). NACA 0012 Starting Impulsively from Rest Pitching from 10° to 30°: $\dot{\alpha}c/2U_\infty = 0.175$; $\tau = 0.6$.

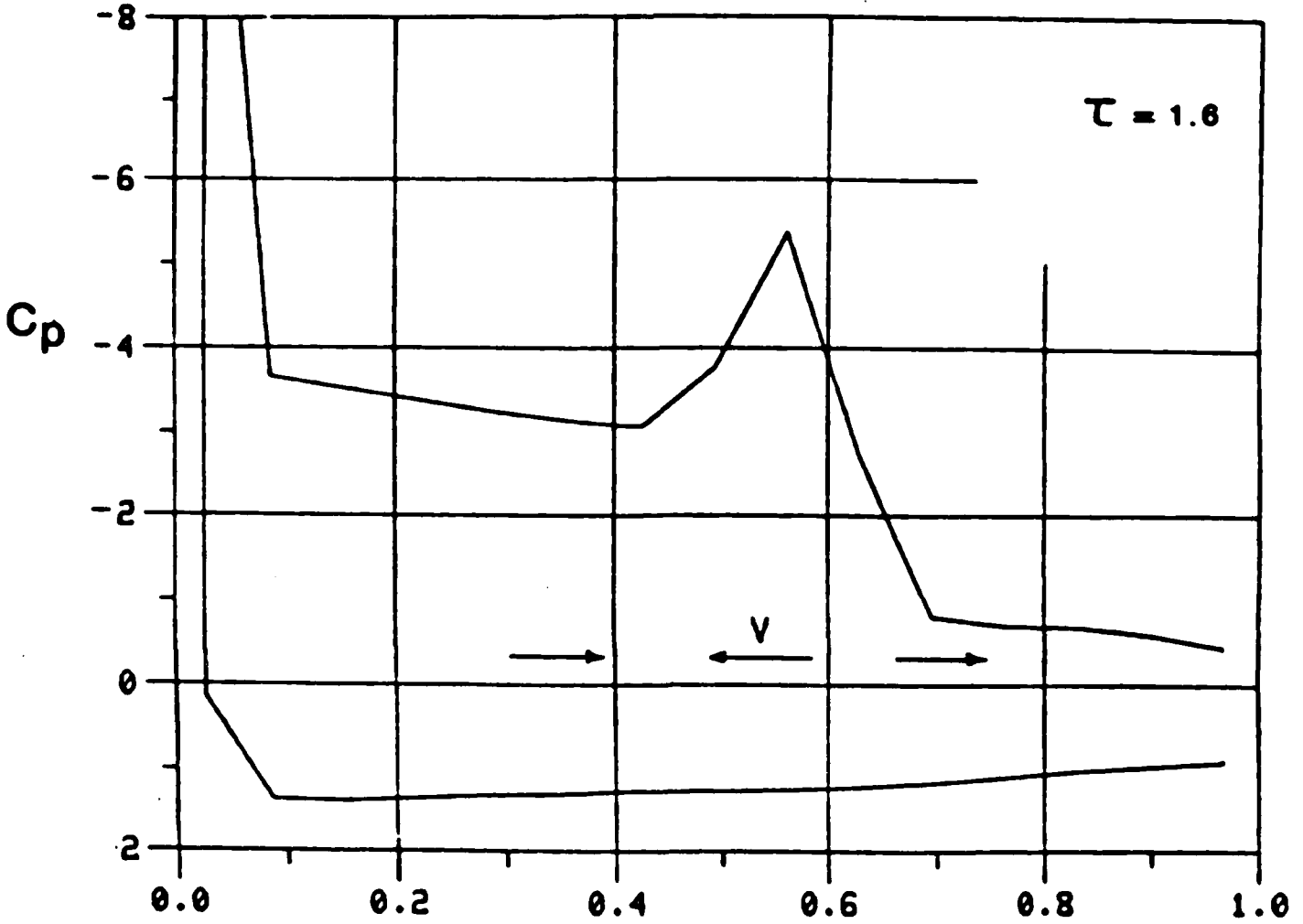

Figure 14(b)(ii). NACA 0012 Starting Impulsively from Rest Pitching from 10° to 30°: $\alpha\dot{c}/2U_\infty$ = 0.175; τ = 1.6.

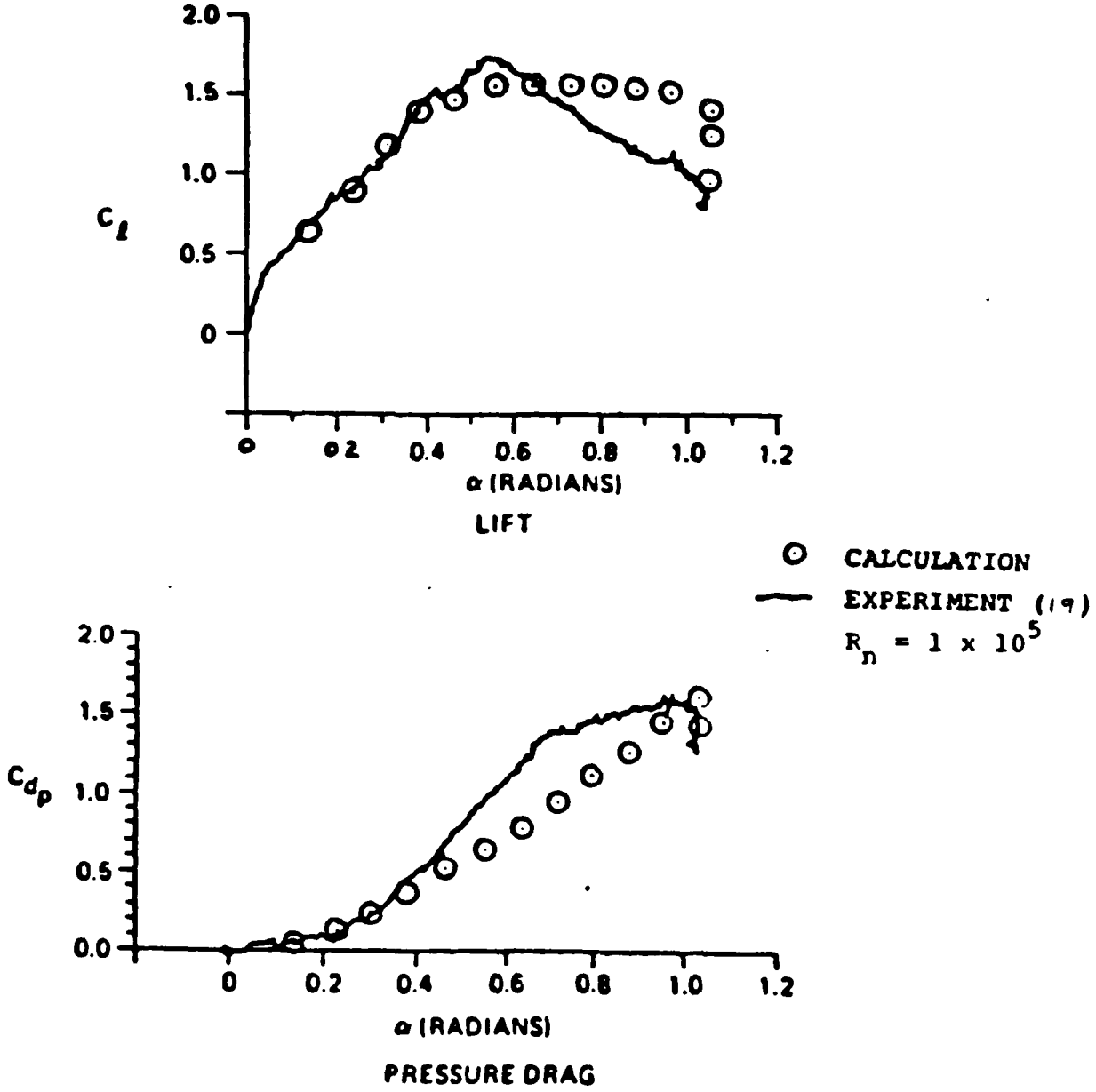

(a) $k = 0.047$, $\alpha_{MAX} = 60°$.

Figure 15. Comparison of Calculated and Measured Lift and Pressure Drag on a NACA 0012 Section During Pitch-up Motion about x/c = .317.

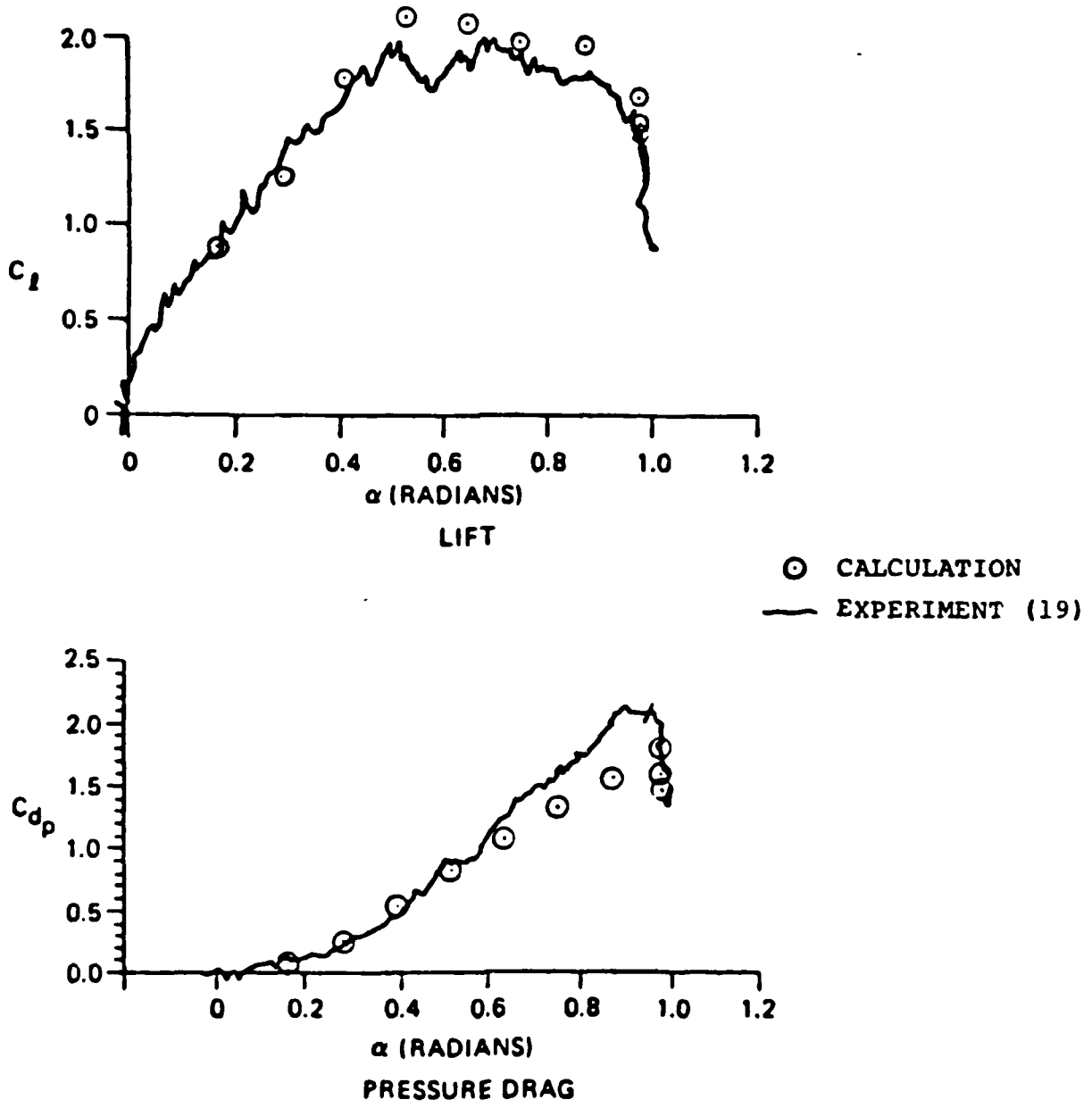

(b) $k = 0.089$, $\alpha_{MAX} = 56°$.

Figure 15. Continued.

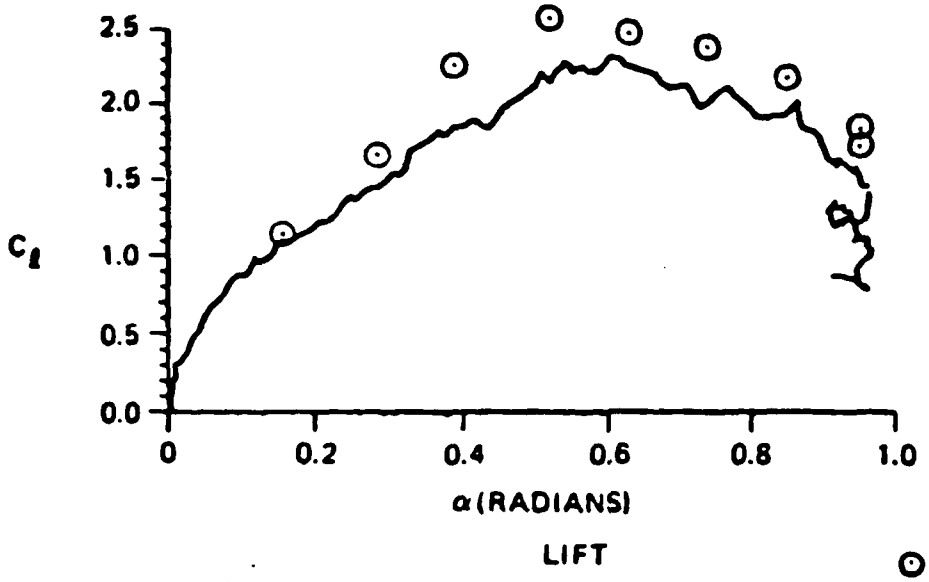

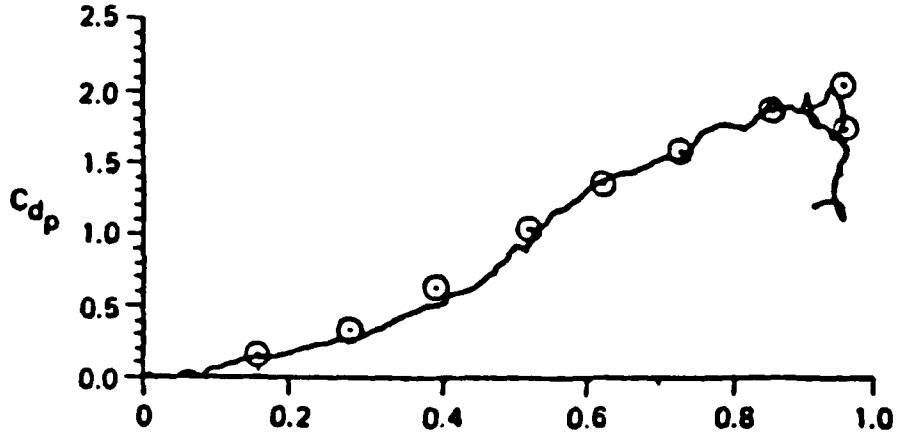

(c) $k = 0.13$, $\alpha_{MAX} = 55°$.

Figure 15. Concluded.

"steady state" conditions to be reached. As stated earlier, because of problems with the amalgamation routine, a strong vortex core did not "condense" for these cases and so the upper surface suction peak seen in the experimental measurements (19) did not materialize; rather, a smeared suction peak appeared because of the more diffuse region of shed vorticity. Consequently, although the integrated lift and drag are in good agreement, the pitching moment characteristic (not shown) is not satisfactory at this time. This upper surface suction peak, which is associated with a reversed flow region under the vortex, was, in fact, computed in earlier preliminary calculations (see Figure 14) involving a high pitch rate, k = 0.175. In this case a vortex core condensed early in the calculation (Figure 14(a)).

Earlier tests of the pitch-up case were repeated with different conditions to compare with more recent data by Helin and Walker (20) at the Seiler Laboratories. Figure 16(a) shows a comparison of wake geometry from two α conditions straddling the α = 45 deg condition of a flow visualization photograph. The wake "boundary" in the calculation shows good qualitative agreement with the photograph. The pitch rate, $\dot{\alpha}c/2V_\infty = 0.2$, and the pitch axis is the quarter-chord line. For the same case a history of the velocity magnitude at an upper-surface point at $x/c = 0.7$ is shown in Figure 16(b) as a function of α. This is in remarkably good agreement with the measurement.

While the two-dimensional program has been used to examine and develop the various routines required for the coupled dynamic separation calculations, the three-dimensional pilot code development has been following closely behind. The unsteady boundary layer calculation--which is performed along computed surface (external) streamlines at each time step--has been fully coupled with the unsteady inviscid program. Test cases have been performed and compared with experimental data from the DFVLR-AVA in Gottingen. These experiments were conducted as part of a cooperative agreement between the DFVLR Institute of Aeroelasticity/West Germany and NASA Langley Research Center. Figure 17 compares the calculated and measured real and imaginary pressure distributions at a 70% spanwise station on an AR = 4 rectangular wing undergoing pitch oscillation about the quarter chord with α = 7.9 deg + 1.0 deg sin (.2t). (Reynolds number is 1.35×10^6.) The potential flow solution is also shown to indicate the extent of the viscous correction. The complete solution is in very good agreement with the measurements. This is still true for the condition, α = 12 deg + 1.0 deg sin (.3t), which is approaching the condition of dynamic stall onset; a pressure deviation is apparent near the leading edge.

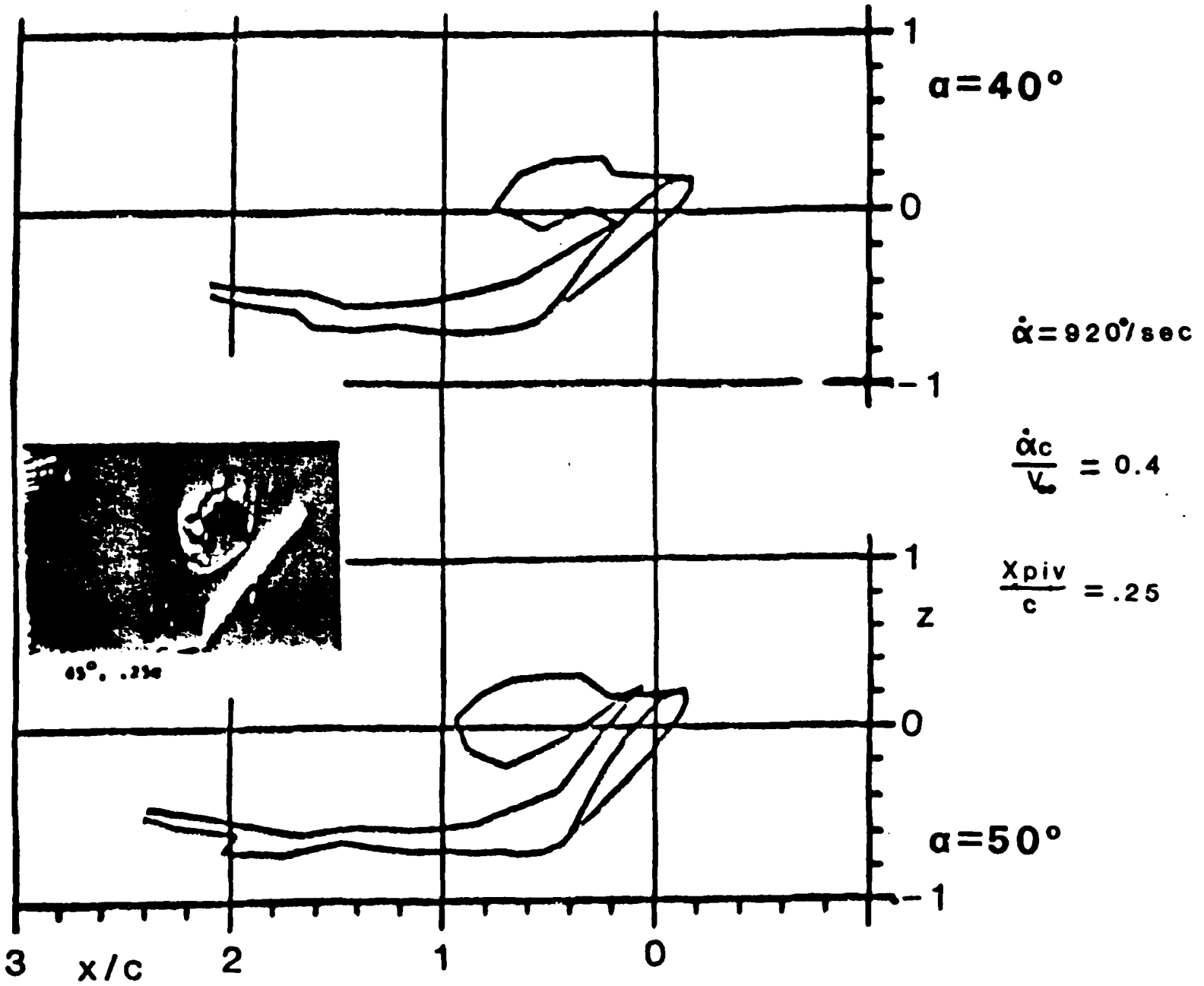

(a) Wake Geometry at Two Time Steps

Figure 16. Comparison with the Pitch-up Data of Helin and Walker (20).

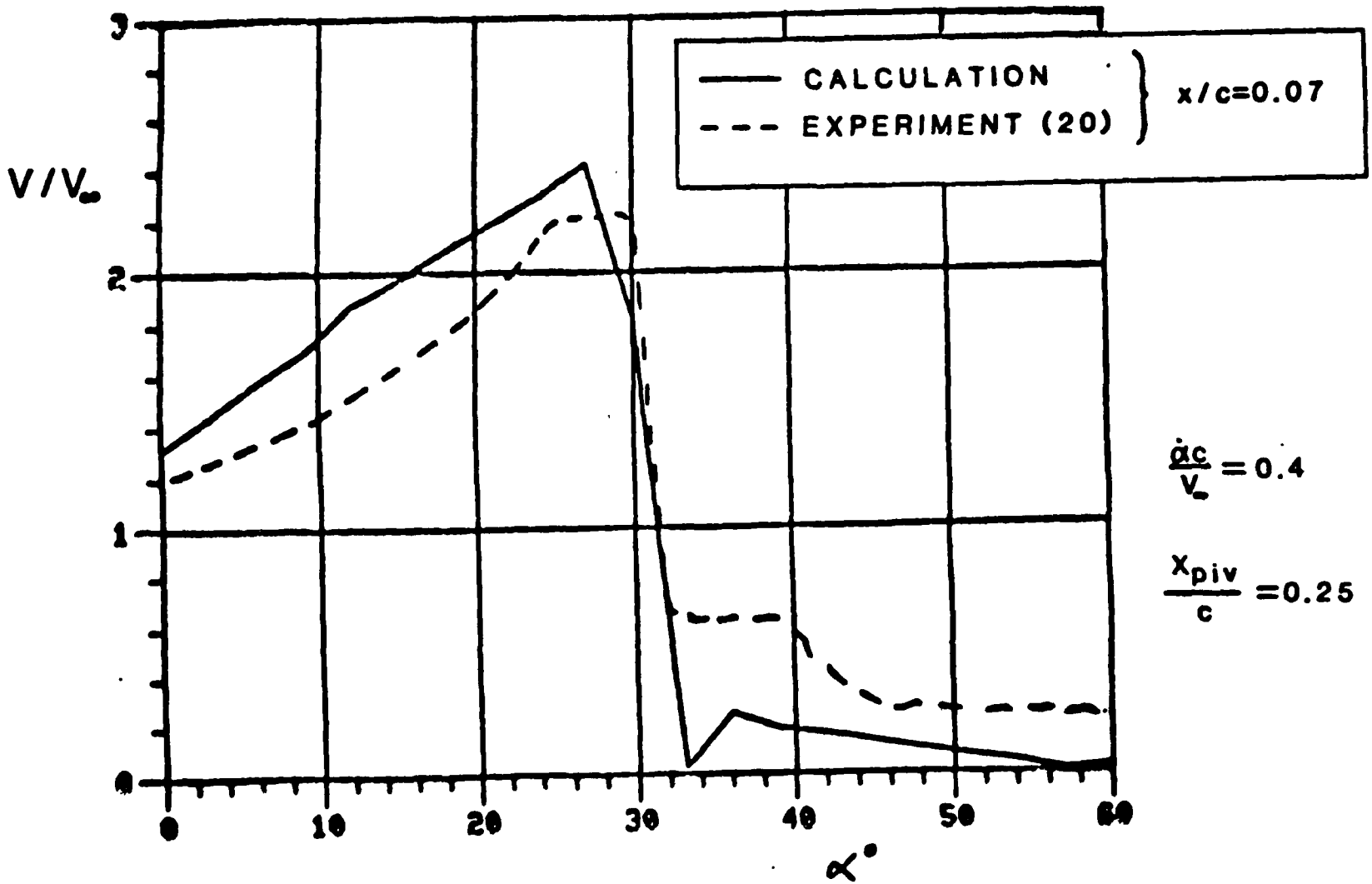

(b) Variation of Velocity at x/c = 0.7 Versus Angle of Attack

Figure 16. Concluded.

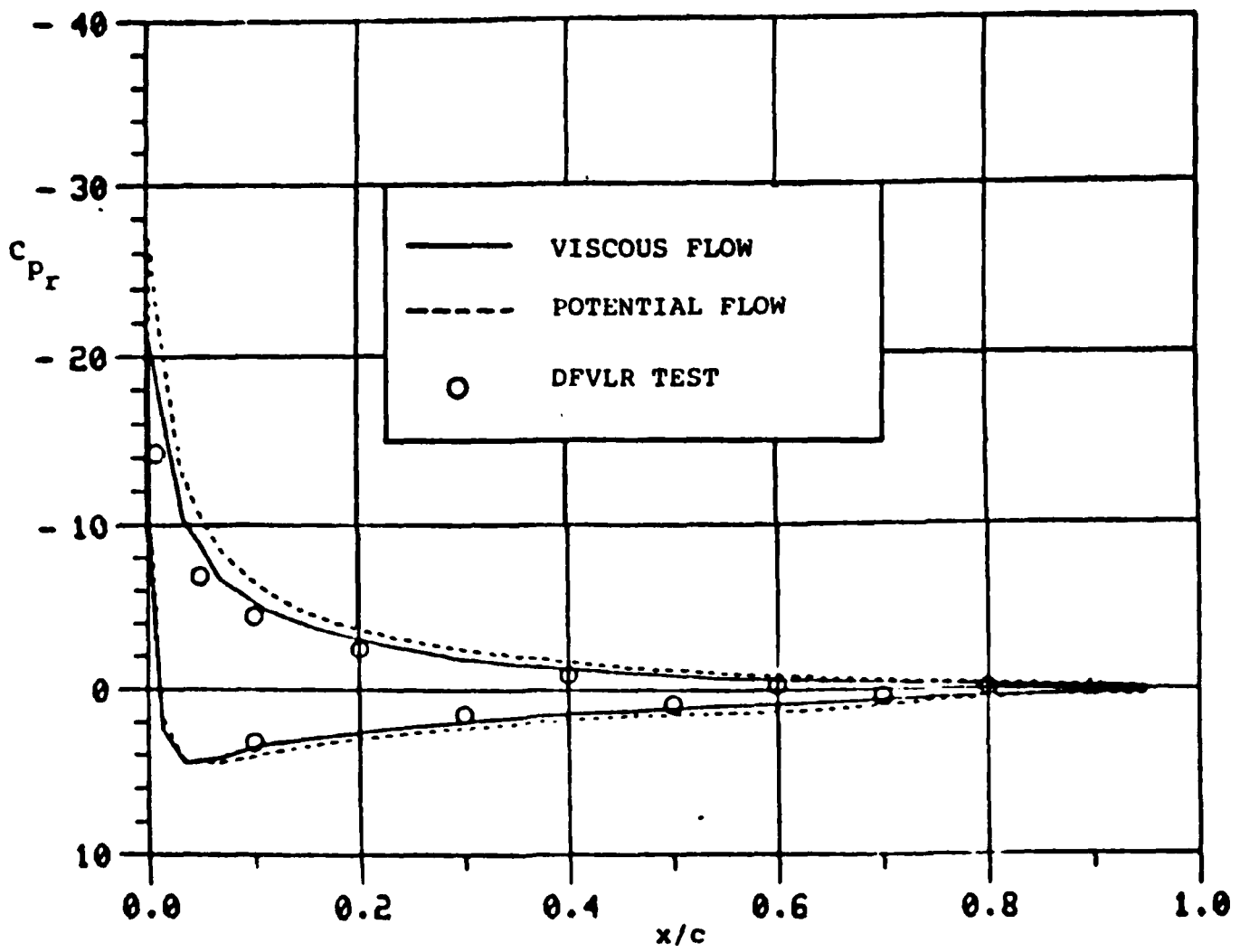

Figure 17(a). Comparison of Chordwise Pressure Distribution (Real Part) at y/s = 0.70 between Computed and DFVLR Data (a_o = 7.9°, a_i = 1°, k = 0.2).

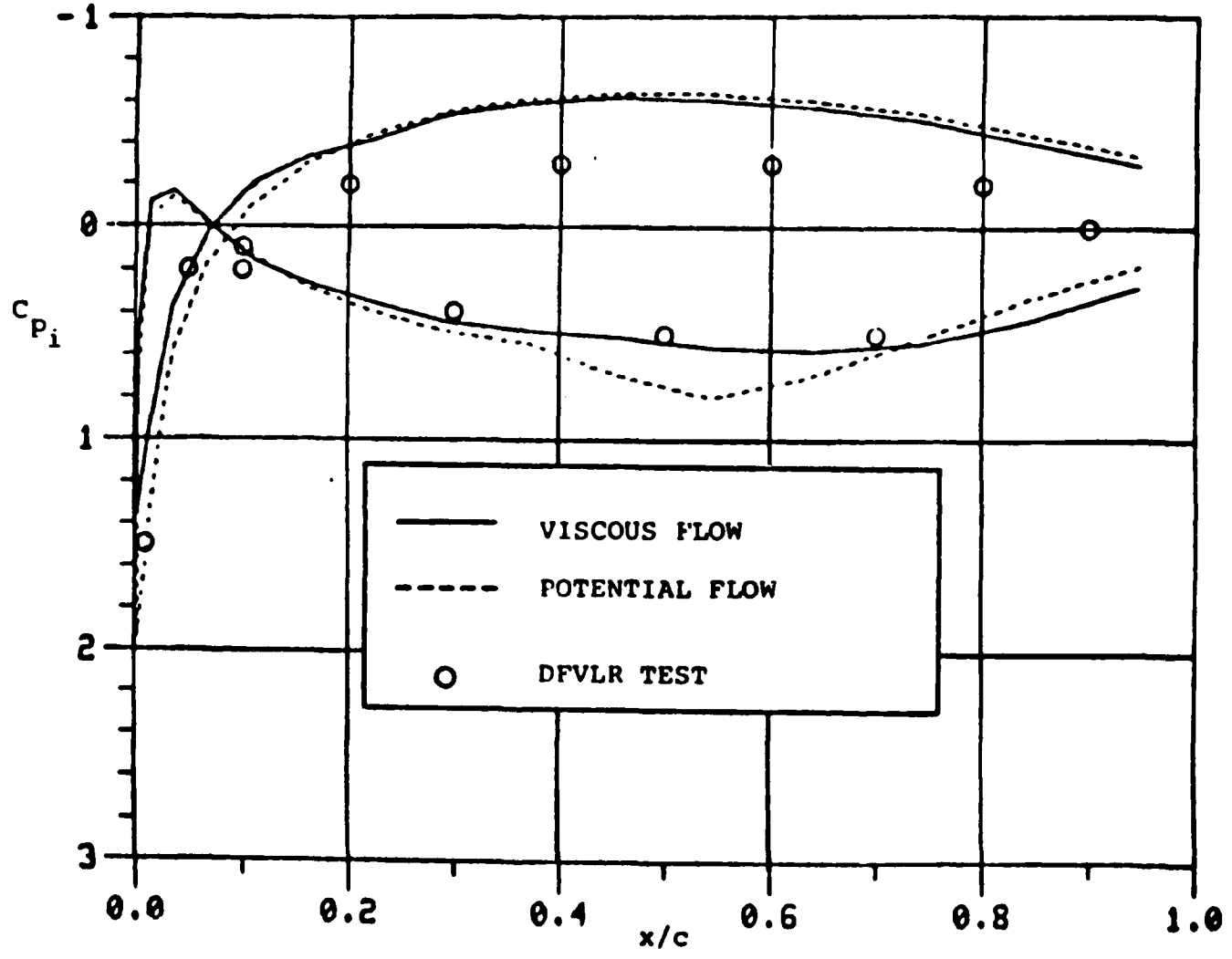

Figure 17(b). Comparison of Chordwise Pressure Distribution (Imaginary Part) at y/s = 0.70 between Computed and DFVLR Data (α_o = 7.9°, α_i = 1°, k = 0.2).

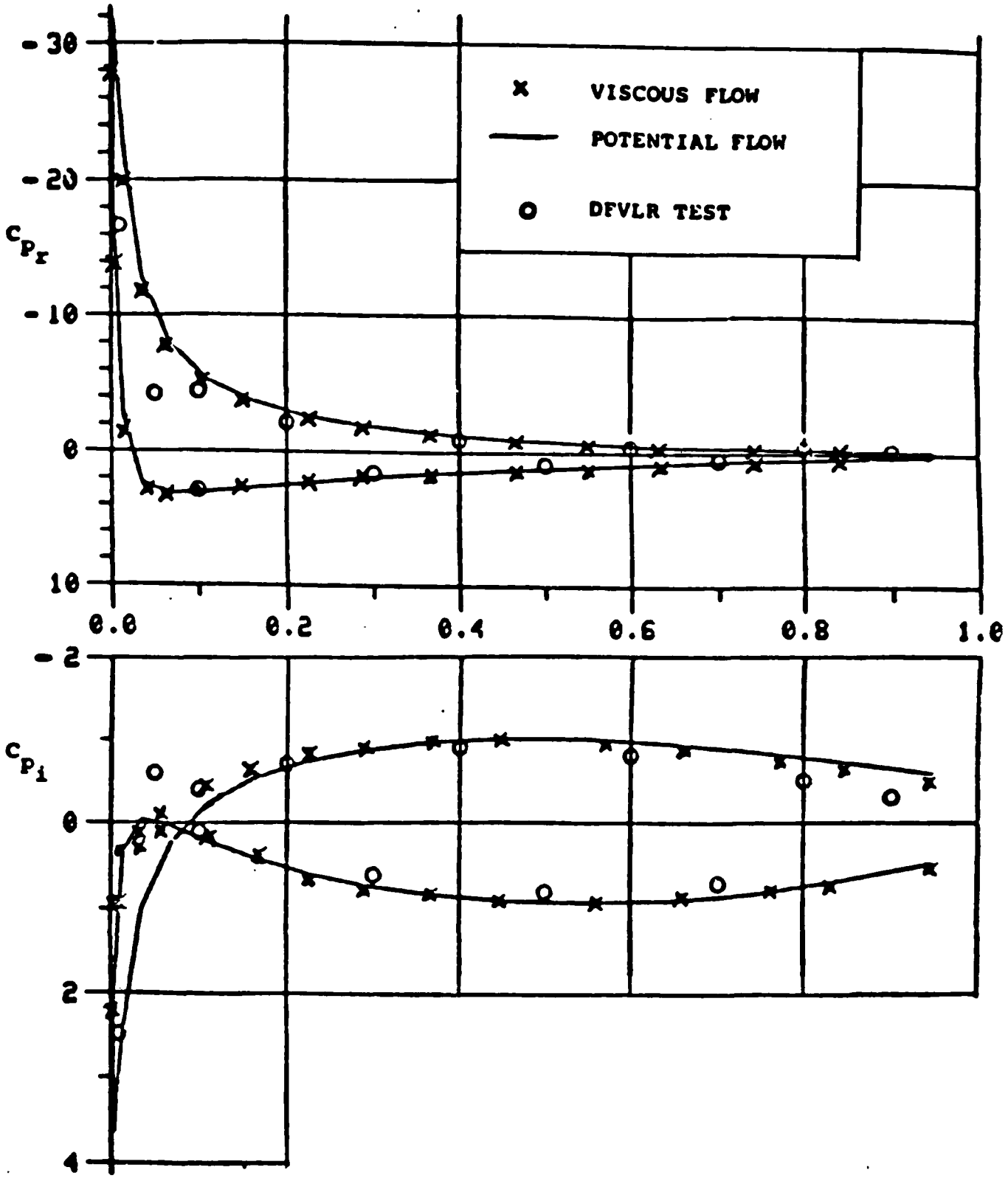

Figure 17(c). Comparison of Chordwise Pressure Distribution between Computed and DFVLR Data (α_o = 12°, α_i = 1.07; k = .3, Rn = 1.35 x 10^6; Spanwise Location, η = 0.7.

5.0 CONCLUSIONS

A system of routines has been developed coupling an unsteady time-stepping potential flow panel code with unsteady integral boundary layer methods. The routines include treatment of the growth of multiple vortex sheets representing free shear layers in the wake. The location of separation, predicted by the boundary layer code, is allowed to move with time. The procedure is completely assembled in a two-dimensional pilot code and shows encouraging results for pitch-up conditions beyond the dynamic stall. Unsteady viscous/inviscid calculations in the three-dimensional pilot code are in close agreement with experimental measurements up to dynamic stall onset.

6.0 REFERENCES

1. Herbst, W., "Supermaneuverability," Proc. Workshop on Unsteady Separated Flow, USAF Academy, August 1983.

2. Lang, J.D. and Francis, M.S., "Unsteady Aerodynamics and Dynamic Aircraft Maneuverability", Paper 29 in AGARD CP-386, May 1985.

3. Laschka, B., "Unsteady Flows--Fundamentals and Applications," Paper 1 in AGARD CP-386, May 1985.

4. Maskew, B., "Prediction of Subsonic Aerodynamic Characteristics: A Case for Low-Order Panel Methods," J. Aircraft, Vol. 19, No. 2, February 1982, pp. 157-163.

5. Maskew, B., Rao, B.M. and Dvorak, F.A., "Prediction of Aerodynamic Characteristics for Wings with Extensive Separations," Paper 31 in AGARD CP-291, September 1980.

6. Maskew, B., "Influence of Rotor Blade Tip Shape on Tip Vortex Shedding--An Unsteady Inviscid Analysis," Paper 80-6 in Proc. 36th Annual Forum of AHS, May 1980.

7. Maskew, B. and Dvorak, F.A., "Prediction of Dynamic Stall Characteristics using Advanced Non-Linear Panel Methods", In Proc. of Workshop on Unsteady Separated Flows, USAF Academy, August 10-11, 1983.

8. McCroskey, W.J., "Recent Developments in Dynamic Stall," Proc. of Symposium on Unsteady Aerodynamics, Univ. of Arizona, Vol. 1, 1975, pp. 1-33.

9. McCroskey, W.J., "Some Current Research in Unsteady Fluid Dynamics -- The 1976 Freeman Scholar Lecture," J. Fluids Engr., Vol. 99, 1977, pp. 8-39.

10. Rehbach, C., "Numerical Calculation of Three-Dimensional Unsteady Flows with Vortex Sheets," AIAA Paper 78-111, Presented at 16th Aerospace Sciences Meeting, Huntsville, Alabama, January 1978.

11. Kandil, O.A., "State of the Art of Nonlinear Discrete-Vortex Methods for Steady and Unsteady High Angle-of-Attack Aerodynamics," AGARD CP-247, 1978.

12. Levin, D. and Katz, J., "Vortex-Lattice Method for the Calculation of the Nonsteady Separated Flow over Delta Wings," J. Aircraft, Vol. 18, No. 12, 1981, pp. 1032-1037.

13. Strickland, J.H., Oler, J.W. and Im, B.J., "Preliminary Results from the Unsteady Airfoil Model USTAR2", Proc. Workshop on Unsteady Separated Flow, USAF Academy, August 10-11, 1983.

14. Geissler, W., "Unsteady Boundary Layer Separation on Airfoils Performing Large Amplitude Oscillations--Dynamic Stall," Paper 7 in AGARD CP-386, May 1985.

15. Cebeci, T., Carr, L.W., Khattab, A.A. and Schimke, S.M., "Computational Aspects of Unsteady Flows", Paper 8 in AGARD CP-386, May 1985.

16. LeBalleur, J.C. and Girodroux-Lavigne, P., "A Viscous-Inviscid Interaction Method for Computing Unsteady Transonic Separation," 3rd Symposium on Numerical and Physical Aspects of Aerodynamics Flows, Long Beach, CA, January 1985.

17. McCroskey, W.J. and Philippe, J.J., "Unsteady Viscous Flow on Oscillating Airfoils", AIAA J., Vol. 13, No. 1, January 1975.

18. McAlister, K.W. and Carr, L.W., "Water Tunnel Visualizations of Dynamic Stall," J. Fluid Engr., Vol. 101, September 1978, pp. 376-380.

19. Francis, M.S., Keese, J.E. and Retelle, J.P., Jr., "An Investigation of Airfoil Dynamic Stall with Large Amplitude Motions", FJSRL-TR-83-0010, F.J. Seiler Research Labs., Air Force Academy, Colorado Springs, CO, 1983.

20. Helin, H.E. and Walker, J.M., "Interrelated Effects of Pitch Rate and Pivot Point on Airfoil Dynamic Stall", AIAA Paper 85-0130, 23rd Aerospace Sciences Meeting, Reno, NV, January 1985.

21. Graham, G.M. and Strickland, J.H., "An Experimental Investigation of an Airfoil Pitching at Moderate to High Rates to Large Angles of Attack", AIAA Paper No. 86-0008, 24th Aerospace Sciences Meeting, Reno, NV, January 1986.

22. Maskew, B. and Dvorak, F.A., "The Prediction of CLMAX using a Separated Flow Model," J. Am. Hel. Soc., April 1978.

23. Curle, N., "A Two-Parameter Method for Calculating the Two-Dimensional Incompressible Laminar Boundary Layer," J. Aero. Soc., Vol. 71, 1967.

24. Cousteix, J. and Houdeville, R., "Singularities in Three-Dimensional Turbulent Boundary Layer Calculation and Separation Phenomena," AIAA J, Vol. 19, No. 8, August 1981.

25. Lyrio, A.A. and Ferziger, J.H., "A Method of Predicting Unsteady Turbulent Flows and its Application to Diffusers with Unsteady Inlet Conditions", AIAA J., Vol. 21, No. 4, April 1983.

26. Hoerner, S.F., Fluid Dynamic Drag, Hoerner Fluid Dynamics, Brick Town, N.J., 1965.

27. McCroskey, W.J., Spalart, P.H., Laub, G.H., Maisel, M.D. and Maskew, B., "Airloads on Bluff Bodies with Application to the Rotor-Induced Downloads on Tilt-Rotor Aircraft," Vertica, Vol. 9, No. 1, 1985, pp. 1-11.

28. McLachlin, B.G. and Karamcheti, K., "Experimental Study of the Flow Field of an Airfoil with Deflected Spoiler," Paper 82-0126, Presented at AIAA 20th Aerospace Sciences Meeting, Orlando, FL, January 1982.

29. McCroskey, W.J., McAlister, K.W., Carr, L.W., Pucci, S.L., Lambert, O., and Intergand, Lt. R.F., "Dynamic Stall on Advanced Airfoil Sections," Paper 80-01, in Proc. 36th AHS Annual Forum, May 1980.

END
DATE
FILMED
JAN
1988